Tampere University

Jesse-Eemeli Viljanen

CONSTRUCTION AND FORMULATION OF CALCULATION MODELS FOR THERMAL SWING ADSORPTION REACTOR MODELLING

Application in Post-Combustion Carbon Capture

Master of Science (Tech.) Thesis
Faculty of Engineering and Natural Sciences
Examiners: Professor of Practice Tero Joronen
University Lecturer Henrik Tolvanen
September 2023

ABSTRACT

Jesse-Eemeli Viljanen: Construction and Formulation of Calculation Models for Thermal Swing Adsorption Reactor Modelling
Master of Science (Tech.) Thesis
Tampere University
Degree Programme of Environmental and Energy Engineering
September 2023

Carbon dioxide capture from combustion-based energy production emissions is one potential method for climate change mitigation and adsorption-based post-combustion carbon capture is currently under research as a potential technology. The main objective of this thesis was to construct and formulate suitable calculation models for the purpose of modelling a thermal swing adsorption reactor in post-combustion carbon capture from flue gas. In the process, the adsorption step would be conducted at a low temperature of 283 K, while the desorption step would include a high temperature carbon dioxide rich purge gas as the desorption medium. The models to be built were chosen to be a one-dimensional Python-based model and a two-dimensional computational fluid dynamics model using Ansys Fluent software with user-defined functions being utilized.

As an initial step, a vast literature review was conducted in order to gain knowledge on the basics of adsorption and adsorption processes, the most important adsorption process parameters and indicators, as well as thermal swing adsorption in the context of post-combustion carbon capture. Literature review also preceded the model construction process, as the heat and mass transfer models for the one-dimensional calculation model and the adsorption isotherm models and parameters for both calculation models were gathered from previous studies in the field.

Following the literature review, the construction process of the calculation models began, which included a significant amount of trial-and-error. First, the one-dimensional model was built, followed by the two-dimensional model. After both models were deemed to represent the behavior of a thermal swing adsorption reactor, the calculations were conducted with relevant data gathered from the calculations.

After the calculations, the data from both models were compared and analyzed. The adsorption step results were considered to be comparable, as the results from the both models were very similar. In the desorption step, however, variation in the results was apparent. The initial carbon dioxide adsorbent loading levels were higher in the two-dimensional model. This was accounted to be due to numerical inaccuracy of the computational fluid dynamics model, which was also further analyzed. The effect of desorption temperature was a key consideration in the modelling work. Desorption temperature level had a significant role on the adsorbent loading levels in the process cycle and the temperature level should be chosen to fit the process needs as a whole.

Thermal swing adsorption -based post-combustion carbon capture possesses many challenges, but it can potentially be utilized to capture at least a part of the carbon dioxide from flue gases. As a conclusion, the objective of constructing the calculation models can be thought to be met, when considering the results as a whole. For future research, the models should be improved and further developed to better represent actual reactor conditions. A two-dimensional Python-based model could provide a highly modifiable modelling tool with computational cost control.

Keywords: thermal swing adsorption, reactor modelling, post-combustion carbon capture, computational fluid dynamics, Python, Ansys Fluent, user-defined function

TIIVISTELMÄ

Jesse-Eemeli Viljanen: Lämpövaihteluadsorption reaktorimallinnuksen laskentamallien rakentaminen ja muotoilu
Diplomityö
Tampereen yliopisto
Ympäristö- ja energiatekniikan tutkinto-ohjelma
Syyskuu 2023

Hiilidioksidin talteenotto polttoon perustuvan energiantuotannon päästöistä on yksi potentiaalinen tapa hillitä ilmastonmuutosta ja adsorptioon perustuvia poltonjälkeisiä hiilidioksidin talteenottomenetelmiä tutkitaan potentiaalisena teknologiana tälle. Tämän diplomityön pääasiallinen tavoite oli rakentaa ja muotoilla sopivat laskentamallit lämpövaihteluadsorptioon pohjautuvan poltonjälkeisen hiilidioksidin talteenoton reaktorimallintamista varten. Prosessissa adsorptiovaihe toteutettaisiin matalassa 283 K:n lämpötilassa ja desorptiovaiheessa korkeassa lämpötilassa oleva korkean hiilidioksidipitoisuuden omaava tuotekaasu toimisi huuhtelukaasuna. Rakennattaviksi malleiksi valittiin yksiulotteinen, Python-koodikieleen perustuva malli sekä kaksiulotteinen, laskennallisen virtausdynamiikan malli Ansys Fluent -ohjelmistolla käyttäjän määrittelemiä funktioita (user-defined function) hyödyntäen.

Työn alkuvaiheessa suoritettiin laaja kirjallisuuskatsaus yleistiedon keräämiseksi adsorptiosta, adsorptioprosesseista, niiden tärkeimmistä parametreista ja indikaattoreista sekä lämpövaihteluadsorptiosta poltonjälkeisen hiilidioksidin talteenoton kontekstissa. Kirjallisuuskatsaus edelsi myös laskentamallien rakentamista, sillä lämmön- ja aineensiirtomallit yksiulotteiseen laskentamalliin ja adsorptioisotermimallit ja -parametrit molempiin laskentamalleihin valittiin aikaisemmista alan tutkimuksista.

Kirjallisuuskatsauksen jälkeen laskentamallit rakennettiin. Mallienrakennusprosessiin sisältyi paljon yritystä ja erehdystä. Yksiulotteinen malli rakennettiin ensin ja sitä seurasi kaksiulotteisen mallin rakentaminen. Kun molempien mallien oltiin todettu edustavan lämpövaihteluadsorptioreaktorin toimintaa, laskennat suoritettiin ja olennainen data laskennoista kerättiin.

Laskentojen jälkeen molempien mallien dataa vertailtiin ja analysoitiin. Adsorptiovaiheen tuloksien todettiin olevan vertailukelpoisia, sillä molemmat mallit tuottivat samankaltaisia tuloksia. Desorptiovaiheen tuloksissa oli kuitenkin huomattavia eroavaisuuksia. Kaksiulotteisessa mallissa alkuvaiheen adsorbenttikuormitus hiilidioksidin osalta oli suurempi. Tämän katsottiin johtuvan numeerisesta epätarkkuudesta, jota analysoitiin tarkemmin. Desorptiolämpötilan vaikutus oli tärkeä näkökulma mallinnuksessa. Tällä lämpötilalla oli suuri vaikutus adsorbentin kuormitustasoihin prosessissa ja lämpötilan valinta tulisikin olla sopiva koko prosessia ajatellen.

Lämpövaihteluadsorptioon perustuvaan poltonjälkeiseen hiilidioksidin talteenottoon liittyy useita haasteita, mutta sitä voidaan potentiaalisesti hyödyntää talteenottamaan vähintään osa savukaasujen hiilidioksidista. Yhteenvetona voidaan todeta, että laskentamallien rakentamisen ja muotoilun tavoite saavutettiin työn aikana, kun laskentatuloksia tarkastellaan kokonaisuutena. Tulevaisuuden tutkimustyötä varten malleja pitää kuitenkin parantaa ja jatkokehittää, jotta ne vastaisivat paremmin oikeita reaktoriolosuhteita. Kaksiulotteinen Pythoniin perustuva malli voisi tarjota monipuolisesti muokattavissa olevan ja laskentakustannuksiltaan hallitun mallinnustyökalun.

Avainsanat: lämpövaihteluadsorptio, reaktorimallinnus, poltonjälkeinen hiilidioksidin talteenotto, laskennallinen virtausdynamiikka, Python, Ansys Fluent, käyttäjän määrittelemä funktio

PREFACE

This thesis was carried out at Tampere University, as a part of Business Finland -funded BioCCU project, with the telos of thermal swing adsorption reactor modelling for carbon capture. Thanks to all the parties and partners involved in the project.

I would also like to thank Professor of Practice Tero Joronen for being the main supervisor and examiner of the thesis and for offering me the thesis opportunity, and University Lecturer Henrik Tolvanen for being the second supervisor and examiner. Both helped me immensely throughout the thesis work, providing assistance and guidance when needed. Special thanks go to Pauli Losoi for tremendous support in the development of the Python-based calculation model and for general process modelling insights, and to Niko Niemelä for the initial spark of interest in computational fluid dynamics and the absolutely necessary help and tips in creating an actual working Ansys Fluent model. Also, thanks to the thesis proofreaders for pointing out mistakes and areas of improvement in the text.

In addition, thanks to the former Tampere University of Technology for providing roots to a unique teekkari culture and the study possibility that has now come to an end for me. Also, thanks to the guild Ympäristöteekkarikilta ry and its members for a warm and welcoming student community of like-minded people. Furthermore, thanks to all the people I met and got to know at Luleå University of Technology during the autumn term of 2022.

Finally, as what comes to those near and dear, I'd like to wholeheartedly express my gratitude to Aleksi Sivonen, Jussi Pesonen, Teemu Uusitalo, Saana Seppälä, Benjamin Rinne, Riikka Määttä, Niklas Pasanen, Halla Kokkonen and Arttu Määttä for being invaluable friends of mine throughout the years, to my mother and father for all the unconditional love and support through my whole life, and for giving me the possibility to call Kuusamo my home, and to Suvi Pauliina Köppä for engineering an exothermic and adiabatic true love process with me. It often goes unsaid, but all of you mean the world to me.

Slide into the water
Become one with the sea
Life seems so much smaller
Swim to the moon
Between the Buried and Me // Swim to the Moon

Hervanta, 6th September 2023

Jesse-Eemeli Viljanen

CONTENTS

LIST OF FIGURES

LIST OF TABLES

GLOSSARY

Abbreviations

1D	one-dimensional
2D	two-dimensional
CO_2	carbon dioxide
D-A	Dubinin-Astakhov (isotherm model)
IUPAC	The International Union of Pure and Applied Chemistry
L/D	length-to-diameter (ratio)
LDF	linear driving force
MOF	metal–organic framework
MTZ	mass transfer zone
N_2	nitrogen
PSA	pressure swing adsorption
SA/V	surface-area-to-volume (ratio)
TSA	thermal swing adsorption
UDF	user-defined function
UDM	user-defined memory
UDS	user-defined scalar
VSA	vacuum swing adsorption

Greek symbols

α	permeability factor	m^2
Δ	change in a specific property or quantity	
ε	porosity	-
λ	isotherm fitting parameter	various units
μ	dynamic viscosity	Pa s
∇	vector differential operator	
Φ	physical adsorption interaction force	

ρ	density	kg m^{-3}
τ	stress tensor	Pa

Latin symbols

a	external surface-area-to-volume ratio	m^{-1}
C_2	inertial resistance factor	m^{-1}
c	concentration	mol m^{-3}
c_p	heat capacity	J kg^{-1} K^{-1}
d	diameter	m
e	Euler's number	
E	energy	J
F	force	N
G	Gibbs free energy	J mol^{-1}
H	heat of adsorption	J mol^{-1}
h	heat transfer coefficient	W m^{-2} K^{-1}
h	enthalpy	J kg^{-1}
J	mass flux	kg m^{-2} s^{-1}
k	mass transfer coefficient	s^{-1}
k	thermal conductivity	W m^{-1} K^{-1}
M	molar mass	kg mol^{-1}
m	mass	kg
P	pressure	bar
p	pressure	Pa
q	adsorbent loading	mol kg^{-1}
q^*	adsorbent equilibrium loading	mol kg^{-1}
S	entropy	J mol^{-1} K^{-1}
S	source term	various units
T	temperature	K
t	time	s
v	velocity	m s^{-1}
z	axial coordinate	m

Subscripts

0	initial condition
e	energy
f	fluid
$f-s$	fluid-to-solid
i	component (adsorbate)
m	mass
p	particle (adsorbent)
s	solid (adsorbent)

1. INTRODUCTION

The world is in turmoil. One of the most prominent reasons for this is human-induced climate change, which can first and foremost be accounted to the vast usage and reliance on fossil fuels in its many forms. Everything needs energy to operate and ever since the Industrial Revolution, fossil fuels have been a dominant source of energy globally. As a result, the humankind has become dangerously dependent on fossil fuels. In 2021, around 80% of the global total energy supply was provided by fossils, namely oil (almost 30%), coal (27%) and natural gas (24%). As for carbon dioxide (CO_2) emissions from fuel combustion, coal usage was responsible for 44%, oil for 32 % and natural gas for 22% of total global emissions. Apart from the years struck by the COVID-19 pandemic, carbon dioxide emissions have been constantly on the rise for decades. (International Energy Agency, 2023b)

Combustion of other carbon-rich fuels, such as biomass-based fuels, also produces carbon dioxide emissions. In Finland the role of biomass in heat and power production is particularly strong. In year 2021 the share of bioenergy of total energy supply was around 30%, accounting for 420 PJ of energy. A large portion of this (377 PJ) was supplied by solid biomass in various forest industries for the energy needs of the processes and in district heating. (IEA Bioenergy, 2023) While biomass-based energy production can be considered to be a form of renewable energy, there is an incentive to reduce carbon dioxide emissions even from such sources. Carbon capture is one of possible ways for minimizing the carbon dioxide emissions of energy production. The total green house gas emissions from fuel combustion in 2021 were 34175.3 Mt_{CO_2eq} (megatonnes of carbon dioxide equivalent) (International Energy Agency, 2023b), while in the same year the total capacity of operational carbon capture and utilisation facilities was around 43 Mt_{CO_2}. From this, only 2.4 Mt_{CO_2} was captured from power production. (International Energy Agency, 2023a)

In general, carbon capture processes in energy production environment can be separated into three distinct types: post-combustion, pre-combustion and oxyfuel combustion capture. In post-combustion capture, carbon dioxide is recovered from the treated flue gas stream. In pre-combustion carbon capture, the solid fuel is first gasified and carbon dioxide is subsequently separated from the resulting synthetic gas stream. Oxyfuel combustion (oxycombustion) utilizes a more oxygen-rich oxidizer than air in the combustion

process. This results in a flue gas stream that is rich in carbon dioxide, while the amount of nitrogen is reduced significantly in comparison with regular flue gas. Post-combustion technology is considered to be the simplest technology to retrofit into an existing thermal heat and power plant, as it does not require extensive modification of the combustion process. (Wilcox, 2012, pp. 16–21)

Various types of post-combustion carbon capture technologies and methods exist. A general distinction can be made between absorption, adsorption and membrane separation. Of these three technologies, absorption is currently the most prominent, accounting for around 57% of current installations. Out of the rest, 14% are based on adsorption, 8% on membranes and 21% on either mineralization or biofixation. (Chao et al., 2021) As chemical absorption has been utilized in gas processing industries for decades, it is an extensively studied and advanced technology. Carbon capture based on chemical absorption has been established in large scale coal power plants in North America (Boundary Dam in Saskatchewan, Canada and PetraNova in Texas, USA). (IEAGHG, 2019, p. 48) However, as Boundary Dam (established in 2014) has been facing challenges related to equipment and suffering from frequent outages (Anchondo, 2022) and Petra Nova (established in 2017) has been offline since 2020 (Mattei & Schlissel, 2022), new technologies and solutions are being sought after.

Adsorption-based carbon capture has attracted attention in recent years and gained interest over absorption with intensive research going on around the numerous aspects of the topic, including the modelling of adsorption phenomena and processes. The problems related to solvent-based absorption capture include toxicity of solvent materials, emission and waste generation, equipment corrosion and high energy requirements. Adsorption is an attractive alternative especially with lower energy requirements and less generated waste in the capture processes. (Ketabchi et al., 2023)

The main objective of this thesis is to construct and formulate suitable calculation models for the purpose of modelling an adsorption-based carbon dioxide capture reactor. Adsorption is to be conducted at a low temperature level, while desorption will be carried out using a carbon dioxide rich product gas at higher temperature. The chosen models to be built are a one-dimensional Python-based model and a two-dimensional computational fluid dynamics model using Ansys Fluent software. Initial literature review is conducted to gain knowledge on adsorption and thermal swing adsorption basics. This is followed by examining prior studies in the field in order to gain further information on the processes, while simultaneously beginning the constructing of the calculation models. Adsorption isotherm models are also gathered from prior studies which are used in the development of the calculation models. When the models are ready to be utilized, the calculations are carried out and relevant data is gathered. After that, the two model results are compared and analyzed. This is followed by drawing up conclusions from the calculation models and results, with potential improvement areas on the models for future research.

Research questions (Q) were set accordingly with a clear-cut research task (T) included, which are:

Q1. Which parameters affect adsorption processes the most and what kind of indicators can be used to evaluate the processes?

T1. Constructing and formulating suitable one-dimensional Python-based and two-dimensional Ansys Fluent calculation models.

Q2. How do the results from the two models compare?

Q3. How significant is the effect of desorption temperature on the process?

Q4. How could the calculation models be further enhanced in future adsorption reactor modelling and research?

The general theory of adsorption and adsorption processes is addressed in chapter 2, in which an answer to the first research question is provided. The results of the research task 1 are not presented directly, but chapter 3 provides insights on the background of the calculation models, as the prior studies utilized in model development and equations used in the models are described in detail. In addition, chapter 4 includes an in-depth description of the materials and methods used, including the model construction procedure. Answers to the second and third research question are provided in chapter 5, where the modelling results gathered from the two models are presented and compared, including the comparison of the three separate desorption temperatures which is of special interest. Finally, an answer to the final research question is provided in chapter 6.

2. ADSORPTION

This chapter covers the fundamental theory of adsorption, including important aspects of adsorption processes. As an introduction, a review of general adsorption phenomena is conducted. Following that, adsorbents and transport resistances concerning adsorption are examined. Finally, some of the most important adsorption process evaluation indicators and the basics of thermal swing adsorption in a post-combustion carbon capture process are covered. Adsorption has many applications but in the scope of this thesis, the main emphasis will be on carbon dioxide capture and the theory covered will be related to the process at hand.

2.1 Adsorption phenomena

Adsorption is defined as a surface phenomenon in which the concentration of a component increases at the surface or interface between two phases. The two-phase combination can be any of liquid-liquid, liquid-solid, gas-liquid or gas-solid. (Noll et al., 1992b, p. 21) The substance that is adsorbed is called an adsorbate (a component capable of being adsorbed is adsorptive) and the material on which adsorption occurs is called the adsorbent. (Noll et al., 1992a, p. 1) Adsorption can be followed by desorption (also called adsorbent regeneration) which is a converse process to adsorption in which the amount of adsorbed substance is decreased on the adsorbent (The International Union of Pure and Applied Chemistry (IUPAC), 2023b).

Adsorption is not to be confused with absorption. By IUPAC's (2023a) definition, in absorption the material (absorbate) is retained by another material (absorbent). In general terms it can be stated that adsorption occurs on the adsorbent surface, whereas in absorption the surface is penetrated. When a clear distinction between adsorption and absorption can not be made, the term sorption (along with sorbent, sorbate and sorptive) can be used. (Thommes et al., 2015) Adsorption, absorption and sorption are illustrated in figure 2.1.

Two different types of adsorption exist, which are physical adsorption (physisorption) and chemical adsorption (chemisorption) (Laidler et al., 2003, p. 931). A comparison between the most important qualities between the two is presented in Table 2.1.

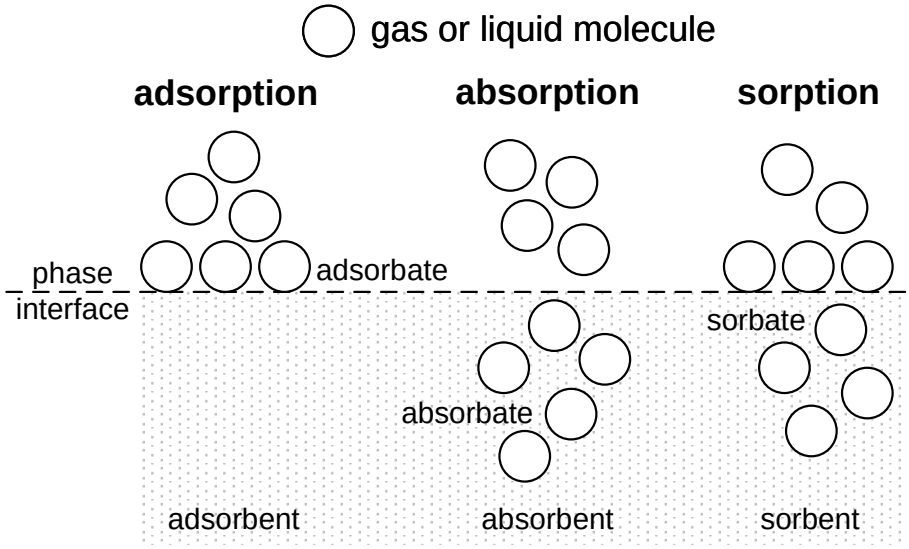

Figure 2.1. *A simple illustration of the differences between adsorption, absorption and sorption. (Rist & Hartmann, 2018; Thommes et al., 2015)*

Table 2.1. *A comparison between the characteristics of physical and chemical adsorption. (Bastos-Neto et al., 2020, p. 2; Laidler et al., 2003, p. 931; Noll et al., 1992b, p. 21; Ruthven, 1984c, p. 29)*

Quantity	Physisorption	Chemisorption
Interactions	Physical (van der Waals)	Chemical (covalent bonds)
Heat of adsorption	<1.5–2 times the latent heat of evaporation	>2–3 times the latent heat of evaporation
Adsorption specifity	Non-specific	Highly specific
Number of layers	Mono- or multilayer	Monolayer
Dissociation of adsorbed species	No	Possible
Temperature range	Low	Wide range
Nature of process	Rapid, non-activated and reversible	Possibly slow, activated and irreversible
Electron transfer	No	Yes

Physical adsorption occurs due to forces that are physical in nature, namely van der Waals (repulsion-dispersion) forces and electrostatic forces (Bastos-Neto et al., 2020, p. 26). On the contrary, in chemical adsorption the forces are chemical in nature as covalent bonds are formed. The heat of adsorption in chemisorption also corresponds to similar values of those in chemical bonds. (Laidler et al., 2003, p. 931) The division between the different interactions in physical adsorption can be made between nonspecific, specific

and adsorbate-adsorbate interactions:

$$\Phi_{total} = \underbrace{\Phi_D + \Phi_R + \Phi_P}_{\text{non-specific}} + \underbrace{\Phi_{F-\mu} + \Phi_{\delta F-Q}}_{\text{specific}} + \underbrace{\Phi_{SP}}_{\text{adsorbate-adsorbate}} \tag{2.1}$$

The non-specificity of dispersion energy Φ_D, close-range repulsion Φ_R and polarization energy Φ_P denote the aspect that the forces always contribute to the total forces. The first two are related to the electric charge distributions while the latter is related to the polarity of the adsorbents. The field-dipole interaction $\Phi_{F-\mu}$ and field gradient-quadrupole interaction $\Phi_{\delta F-Q}$ forces are specific, requiring adsorbate molecules to exhibit permanent dipole and quadrupole forces. If none are present, these specific forces are zero, which is also the case for nonpolar adsorbents. The self-potential Φ_{SP} is caused by adsorbate-adsorbate interactions between separate adsorbate molecules. The higher the adsorbate coverage, the higher the interaction force. (Sherman, 1991, pp. 530–531)

Adsorption selectivity is strongly linked to the molecular forces. The polarizability, dipole moment and quadruple moment of adsorbates are often a good indication of the magnitude of adsorption for certain molecules on different adsorbent types. The relative polarizability and the electric field strength of an adsorbent surface are the main factors in determining the adsorption strength of an adsorbate molecule. (Sherman, 1991, pp. 532–533) A potential energy curve diagram for representing the relationship between physical and chemical adsorption is presented in figure 2.2.

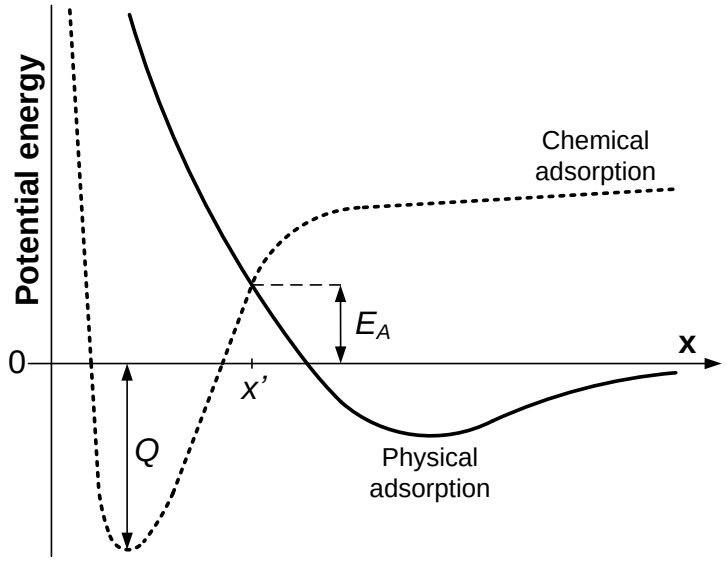

Figure 2.2. *Potential energy diagram for physical adsorption of a molecule and chemical adsorption of two atoms. Q is the potential energy, E_A the activation energy and x is the distance from the adsorbent surface. Adapted from Barbato & Bruno (1996, p. 6).*

The potential energy curves are related to the heats of adsorption, as the potential energy minimums of physical adsorption in specific adsorbate-adsorbent pairings correlate well with the heats of adsorption. In addition, the potential energy minimums also corre-

spond to the strength of the bonds, with the bonds formed in chemical adsorption being more powerful. Adsorption processes are almost exclusively exothermic, while desorption processes are endothermic, however some chemical adsorption processes have been deemed to be endothermic by Thomas (1961). The exothermic nature of physical adsorption leads to heat release. The Gibbs free energy change equation can be used to describe the phenomenon:

$$\Delta G = \Delta H - T\Delta S \tag{2.2}$$

For adsorption to occur, the change in Gibbs free energy ΔG has to be negative. Here the change in entropy ΔS is negative due to adsorption, as the gas molecules are more ordered on the adsorbent than in the bulk gas phase (losing at least one degree of freedom). Similarly, the change in enthalpy ΔH is also negative, leading to the release of heat when adsorption occurs. As the term $T\Delta S$ is positive, the magnitude of ΔG is affected by the temperature. Lower temperature levels lead to lower values of ΔG, resulting in stronger adsorption. The opposite applies to desorption, as higher temperatures lead to more efficient desorption. (Sherman, 1991, p. 534; Thomas & Crittenden, 1998b, p. 32)

Both of the adsorption processes are spontaneous but chemical adsorption has a certain, potentially substantial activation energy E_A, as depicted in figure 2.2. This means that chemical adsorption may require higher temperatures in order to be activated compared to temperatures required by physical adsorption. (Barbato & Bruno, 1996, pp. 5–6) As the heat of adsorption and potentially temperature levels in chemical adsorption are higher than in physical adsorption, the indication is that the energy needed for desorption, in order to recover the adsorbed species, is also higher for chemical adsorption than for physical adsorption (Abd et al., 2020). In relation to process design, the high energy requirement subsequently leads to rising capital costs and decreasing process efficiency. According to Laidler et al. (2003, pp. 932–933), in a chemical adsorption process the physical adsorption is a precursor step and it accounts for the lower activation energy needed for the chemical adsorption to occur. This also means that physical adsorption is always the favored process of the two. In the scope of this thesis, as the carbon dioxide capture process is based on physical adsorption, chemical adsorption will not be further discussed.

2.2 Adsorbents

Adsorbent materials exist in various types, but a general requirement for an adsorbent material of any form is an easily accessible high internal volume coupled with high internal surface area for adsorptive materials to be adsorbed onto. Internal surface area (expressed in square meters per a gram of adsorbent material) usually varies between 100–3000 $m^2\,g^{-1}$. However, in practice the range is limited to around 300–1200 $m^2\,g^{-1}$. In

addition, good mechanical properties to prevent breakdown along with kinetic properties for rapid adsorption and desorption are also required. Material price is also a major consideration to be taken into account, especially when designing industrial-scale adsorption processes. (Thomas & Crittenden, 1998a, p. 8) In the context of carbon dioxide adsorption, along with the mechanical strength of the adsorbent and cost, some additional important criteria for the choice of a suitable adsorbent are adsorbent adsorption uptake capacity, selectivity and heat of adsorption. (Abd et al., 2020)

Adsorbents used in carbon dioxide capture can generally be divided into two distincs types, carbonaceous adsorbents and non-carbonaceous adsorbents. Carbonaceous adsorbents include activated carbons, carbon molecular sieves, carbon nanotubes and graphene. Non-carbonaceous adsorbents on the other hand include materials such as zeolites, silica-based materials and metal–organic frameworks (MOF). (Abd et al., 2020) Another way of classifying adsorbents is traditional materials, such as activated carbon and silica gel, and more developed materials, such as zeolites. Traditional materials usually exhibit a variation in the distribution of pore sizes, while in materials like zeolites the crystal structure of the adsorbent material determines the micropore sizes and there may not be a clear pore size distribution at all. (Ruthven, 1984a, p. 4) In terms of physical adsorption, the adsorbent pore sizes can be classified as

- macropores (>50 nm in diameter),
- mesopores (2–50 nm) and
- micropores (<2 nm).

The listed sizes above are all categorized under nanopores (<100 nm). Micropores can also further distinguished into wide micropores (supermicropores) and narrow micropores (ultramicropores). (Thommes et al., 2015) A graph of typical pore size distributions for various zeolite types and carbon-based adsorbents is presented in figure 2.3.

Depending on the adsorbent material, the pore sizes and their distributions can vary greatly. As activated carbons are often manufactured from various natural carbonaceous materials with thermochemical conversion processes, the pore size distribution can only be controlled to a certain degree. Zeolites, on the other hand, can be both natural and synthetic. The pore size distribution of synthetic zeolites and other synthetic adsorbents can be controlled to a very high degree. (Thomas & Crittenden, 1998a, pp. 14–15, 24)

2.3 Transport resistances in adsorption

Adsorption and desorption are dynamic phenomena that are not ideal and include numerous resistances that affect the respective rates. According to Thomas & Crittenden (1998c, p. 67), the resistances are identified as:

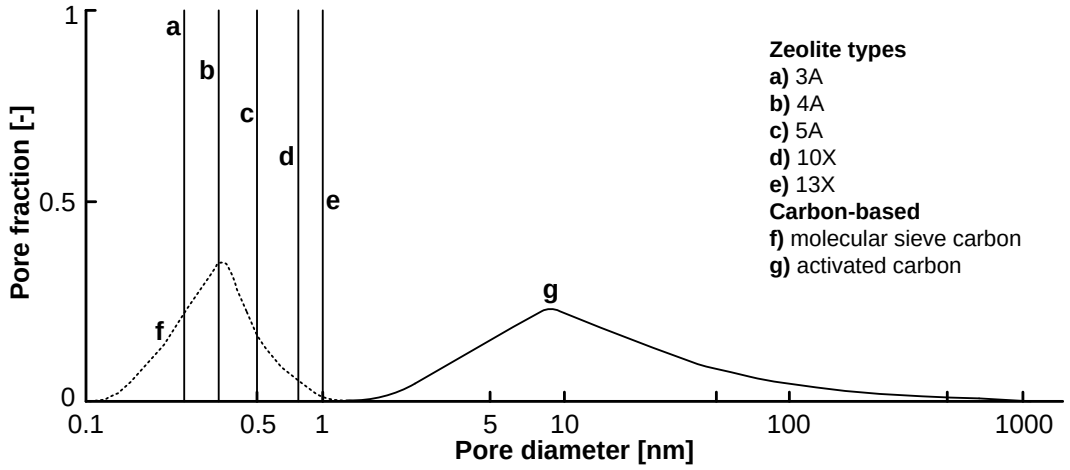

Figure 2.3. *Pore size distribution diagram of certain zeolite and carbon-based adsorbents. Pore sizes vary in carbon-based adsorbents while zeolites have uniform pore sizes. Adapted from Thomas & Crittenden (1998a, p. 10).*

1. Interparticle (between adsorbate and adsorbent) mass and heat transport
2. Macropore or micropore diffusion
3. Intracrystalline diffusion (mainly zeolite and silicalite adsorbents)
4. Surface diffusion (in parallel with macropore and micropore diffusion)
5. Particle interior heat transfer (related to adsorption exothermicity)

From this listing, number 1 occurs externally to adsorbent particles (interparticle) while numbers 2–5 occur within said particles (intraparticle). In the context of physical adsorption, intraparticular resistances are controlled almost exclusively by mass transfer resistances while interparticular resistances are conversely controlled by heat transfer resistances. The ultimate relationship between resistances depends on the adsorbate-adsorbent pairing and process conditions. (Thomas & Crittenden, 1998c, pp. 67–68, 82–83) Figure 2.4 illustrates a simplified adsorbent particle and the mass transfer resistances associated with it, along with flow-related affecting factors.

Interparticle mass and heat transport resistances have been noted to be the most dominant rate limiting factors. Interparticle transport rates are limited by a layer of fluid that covers the whole area of an adsorbate particle, which can also be described as a heat and mass transfer boundary layer. When determining the adsorption rates, this layer is taken into account in the definition of heat and mass transfer coefficients. The difference in temperature (heat transfer) or concentration (mass transfer) between the particle surface and bulk fluid is applied as a linear driving force. (Thomas & Crittenden, 1998c, pp. 67–69) Axial dispersion, which can also have an effect on the transfer phenomena, can be characterized as the back mixing and bulk fluid element diffusion in the axial direction of the stream (Bahadori, 2012). The effect is especially present in smaller, laboratory-scale experiments. However, in certain industrial-scale applications with high velocities and

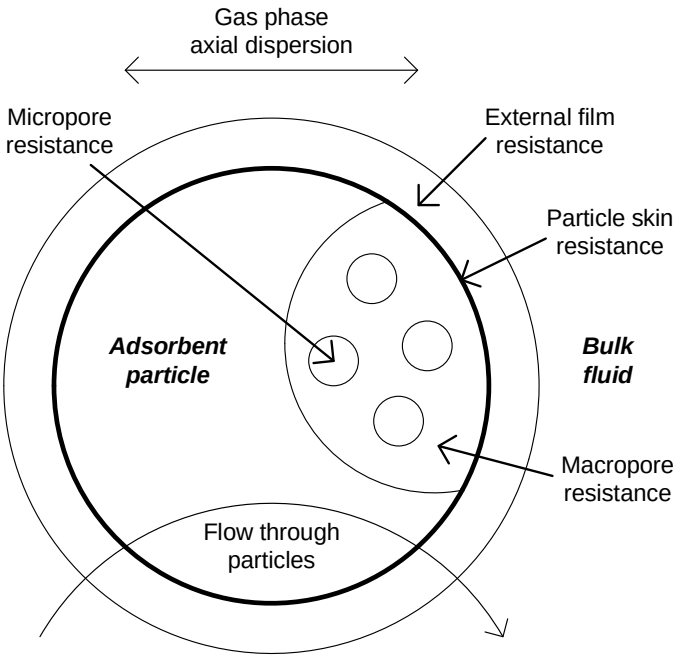

Figure 2.4. *Mass transfer resistances in adsorption, including additional flow-related factors (axial dispersion and flow through particles). Adapted from Thomas & Crittenden (1998a, p. 9).*

large reactors the effect of axial dispersion often need not be taken into account (Froment et al., 2010, pp. 708–709).

The effects of macropore and micropore diffusive fluxes depend on the pore size distribution of the adsorbent particles and the mean free path (the distance the adsorbate molecules travel on average between molecular collisions) of adsorbate molecules. If the mean free path is substantial in comparison to the pore size, micropore diffusion (molecules colliding with the pore walls) occurs. (Ruthven, 1984d, p. 136) On the contrary, if the pore size is larger in comparison to the mean free path, macropore diffusion (collisions between molecules in the gas phase of the pore) is the diffusive flux to take effect (Thomas & Crittenden, 1998c, p. 70). There are many separate forms of macropore diffusion, of which the most prominent ones are bulk molecular diffusion, Knudsen diffusion, Poiseuille flow and surface diffusion. In a gas or a vapor phase, Knudsen and surface diffusion can be in many cases the most prominent forms of diffusion. (Bastos-Neto et al., 2020, p. 17).

Surface diffusion can be caused by the already-adsorbed adsorbate molecules if the molecules possess enough mobility (not prevented by attractive forces) on the adsorbate site by moving from an adsorption site to another. Occurence of surface diffusion is in parallel with bulk molecular and Knudsen diffusion and therefore it can not be measured directly. For surface diffusion to be of any significance, a notable amount of physical adsorption, when the adsorbed layer is prominent on the adsorbate molecule, is needed

as a prequisite. (Ruthven, 1984d, p. 137; Thomas & Crittenden, 1998c, p. 74)

2.4 Adsorption equilibrium

In order to successfully analyse, design and model adsorption systems and processes, equilibrium data is essential. Equilibrium data provides information on the specific adsorbate in terms of adsorption capacity on a certain adsorbent. This information is normally presented in diagrams, either in the forms of isotherms (adsorbed amount against pressure with constant temperature), isobars (adsorbed amount against temperature at constant pressure) or isosteres (logarithm of pressure against the inverse of temperature at constant adsorbed amount) (Bastos-Neto et al., 2020, p. 6). A graphical presentation of these diagrams is shown in figure 2.5.

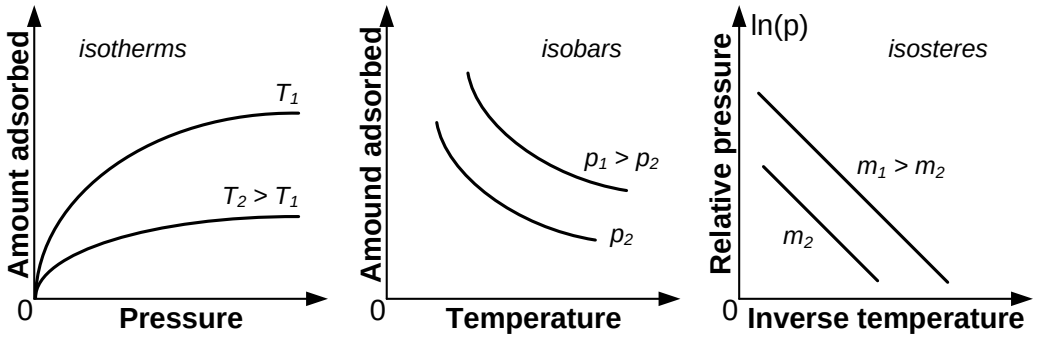

Figure 2.5. *Adsorption equilibrium data presented in the form of isotherms, isobars and isosteres. Adapted from Keller & Staudt (2005, p. 361) and Bastos-Neto et al. (2020, p. 6).*

Of these three diagrams, the isotherm form is the most commonly used one. It is important to note that adsorption and desorption processes are not outright isothermal, despite the isotherm projection, as heat and mass transfer rates may be preventing purely isothermal behaviour of the processes (Thomas & Crittenden, 1998c, pp. 82–83). In terms of thermodynamics, an adsorption isotherm is the thermal equation that describes the behavior of the adsorbed phase, being a function of pressure, temperature and the mass of the adsorbent material. As modelling adsorbate-adsorbent interactions using molecular methods is a very complex and difficult task, a more practical approach can be taken with the utilization of adsorption isotherms. The choice of a correct isotherm provides information on the characteristics of porous adsorbent materials and aids the design of adsorption processes. (Keller & Staudt, 2005, pp. 359–360) By IUPAC's (2015) definition, physical adsorption isotherms can be classified into eight different types. These isotherm types are presented in figure 2.6.

Albeit a number of different isotherm types exist and all of them are encountered in various adsorption processes, isotherm types I, II and IV are the most common ones (Thomas &

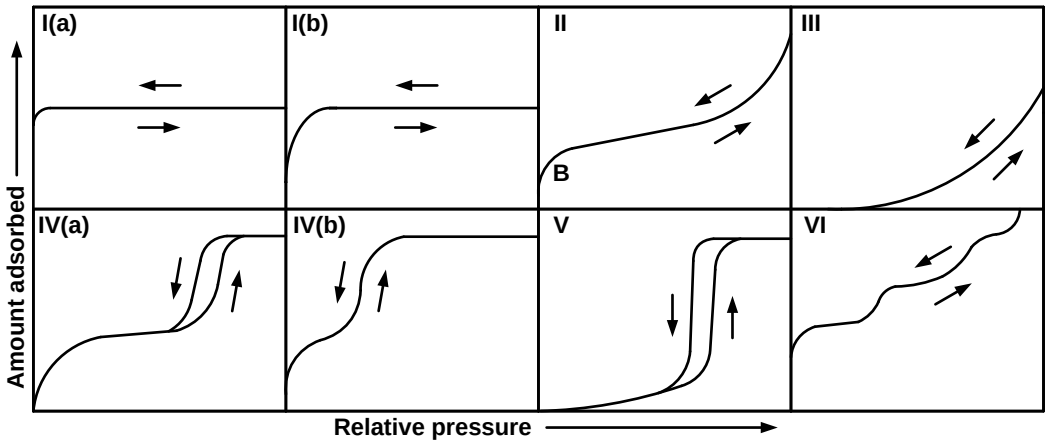

Figure 2.6. *Different types of physical adsorption isotherms according to IUPAC, indicating the behaviour of an adsorbent-adsorbent pair. Arrows pointing to right or up indicate adsorption while arrows pointing to left or down indicate desorption. Adapted from Thommes et al. (2015).*

Crittenden, 1998b, p. 33). Data gained from experiments can be compared with the classified isotherms in order to identify which isotherm represents the behavior of a certain adsorbate-adsorbent pairing. Various mathematical models and theories have been developed in order to describe equilibrium data and accurately model adsorption processes. Mathematical models exist both for single- and multi-component adsorption systems.

2.5 Adsorption dynamics

Two important indicators in adsorption processes are mass transfer zone (MTZ) and breakthrough curves. Micro and macro approach are two perspectives that can be taken in terms of mass transfer. Micro approach concentrates on the mathematical models and equations behind mass transfer with specified mass transfer coefficients and diffusion models. Macro approach portrays a more practical point of view in MTZ. (Anderson, 1977, p. 183) A MTZ progresses through the length of the adsorbent bed while mass transfer only occurs within the MTZ and adsorbate loading increases. Eventually, as the adsorbent bed reaches equilibrium and no more adsorption occurs, MTZ ceases to exist. A breakthrough curve can be used to characterize the equilibrium point of the adsorbent bed. (Thomas & Crittenden, 1998d, pp. 102–103) Figure 2.7 depicts the breakthrough curve and the MTZ in a fixed-bed adsorption column for a single-component adsorption system.

When an adsorption process progresses to time t_b, breakthrough occurs and the amount of adsorbate in the effluent starts to increase and by t_{sat} the adsorbate concentration in the effluent has increased from c (initially 0) to inlet concentration of c_0, as can be seen from Subfigure 2.7a. At this point no more adsorption occurs and the whole adsorbent bed is at equilibrium. The breakthrough concentration can be defined to suit the needs

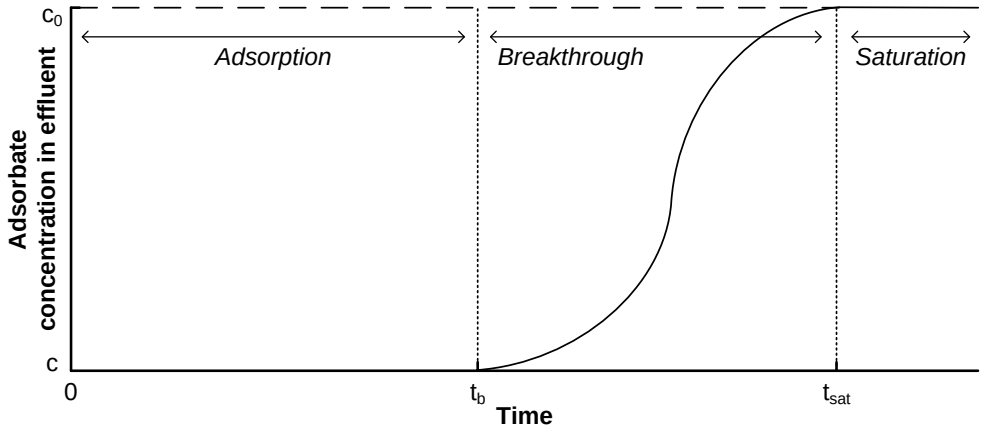

(a) *A breakthrough curve, which represents the increase of adsorbate concentration in the effluent as the adsorption capacity of the adsorbent bed diminishes.*

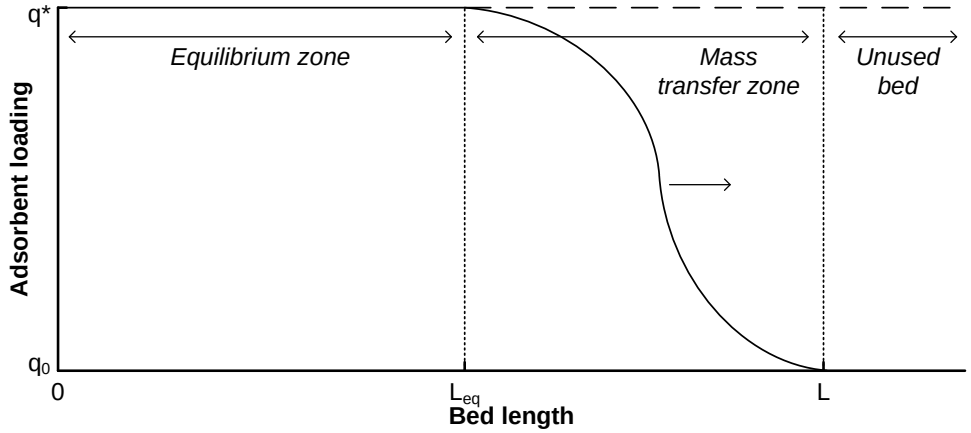

(b) *A mass transfer zone, which moves in the bed as adsorption progresses until adsorbent loading reaches maximum in the whole bed and adsorption ceases.*

Figure 2.7. *Depiction of a breakthrough curve and mass transfer zone for a single-component in a fixed-bed adsorption column. Note that the graphs depict separate time steps of a process. Adapted from Anderson (1977, p. 185) and Thomas & Crittenden (1998d, p. 104).*

of the design, for example as the minimum amount of adsorbate that is detected or as the maximum amount of adsorbate that is allowed in the effluent. (Anderson, 1977, pp. 184–186) In practical applications, the desorption step often needs to be initiated before breakthrough t_b in order to gain satisfactory adsorption results, as adsorption efficiency starts to decrease after breakthrough occurs. Subfigure 2.7b represents a moving MTZ in the adsorption column. The MTZ is essentially of length between L_{eq} and L until the adsorbent bed reaches equilibrium concentration q^* with the adsorbate and no more mass transfer occurs. (Thomas & Crittenden, 1998d, p. 103) In general, breakthrough occurs when the edge of MTZ at length L reaches the edge of outlet in the bed and no more unused bed is available (Anderson, 1977, p. 184).

For a multi-component system, the breakthrough curve can be different for each adsorbate component. For the adsorbate that is adsorbed weaker, a so-called roll-up or roll-

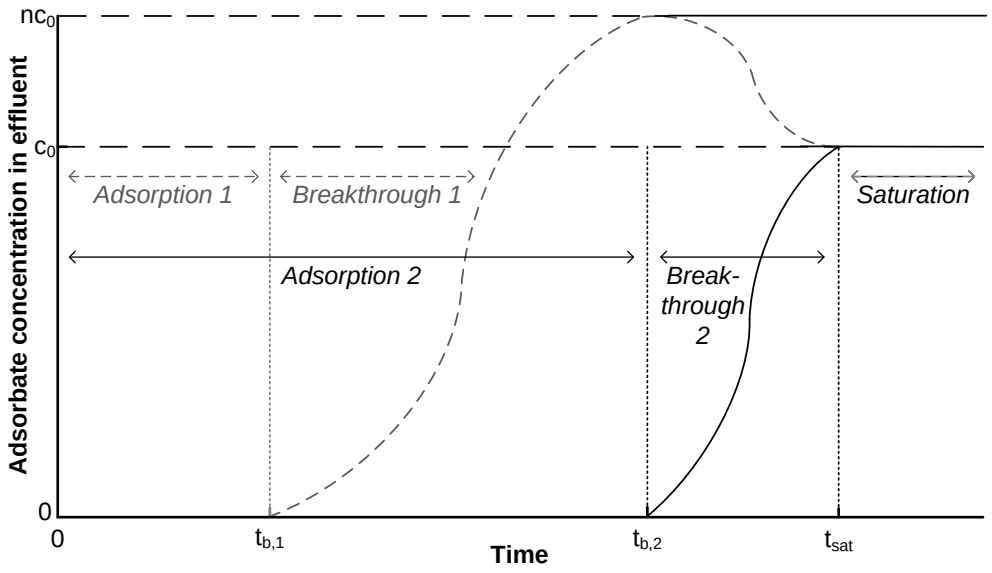

Figure 2.8. *A breakthrough curve for a dual-component adsorption process, depicting the roll-over phenomenon for the weaker adsorbate (component 1). Adapted from Anderson (1977, p. 185), Thomas & Crittenden (1998d, p. 104) and Roy & Moharir (2019).*

over can occur, which is depicted in figure 2.8. (Kapoor & Yang, 1987) Initially, as breakthrough begins for component 1, at some point the outlet concentration for component 1 will be higher than the inlet concentration of the component. This is due to the fact that while the bed has already saturated for component 1 (occurs as concentration of component 1 reaches inlet concentration c_0), adsorption of component 2 still progresses. As a result, only component 1 leaves the bed and the resulting concentration (and mole fraction) at the outlet is higher. The roll-over leads to the outlet concentration to be higher than the inlet concentration (indicated by nc_0). When component 2 also reaches breakthrough, the concentration of component 2 at the outlet starts to increase and the concentration of component 1 starts to decrease. Finally, when component 2 reaches its saturation point, the whole bed is fully saturated with both components and the outlet concentrations of both components equals the inlet concentrations as no more adsorption occurs. (Kapoor & Yang, 1987)

In the case of carbon dioxide adsorption from a flue gas stream, for bulk components such as nitrogen and carbon dioxide, the breakthrough curve for component 1 would represent the breakthrough behavior of nitrogen. This is because carbon dioxide is expected to be the adsorbate component of interest and the adsorbed amount to significantly exceed the adsorbed amount of nitrogen. Therefore, as the adsorption of carbon dioxide takes longer, the breakthrough for carbon dioxide occurs later than the nitrogen breakthrough. Thus the adsorption of carbon dioxide is assumed to follow the behavior of component 2.

2.6 Thermal swing adsorption in post-combustion carbon capture

As an adsorbent has limited adsorption capacity, it will eventually need to be either regenerated or disposed. As disposal is often not an option from an economical standpoint, it leads to the need to design an adsorption process that includes desorption. Adsorption can be conducted in either fixed-bed or moving bed configurations as either cyclic batch or continuous processes. The modelling procedure in this work concentrates on a cyclic fixed-bed batch reactor process and therefore moving bed reactors and continuous processes will not be discussed in detail. The pros of a fixed-bed system include simple equipment which are economic to manufacture, along with less wear on the adsorbent material compared to a moving bed system. Cons include the need for a separate column or columns when a saturated adsorbent needs to be regenerated, possible challenges in achieving satisfactory heat transfer in bed cooling and difficulty in rigorous design of full-scale processes. (Thomas & Crittenden, 1998d, pp. 96–98)

Desorption method distinguishes the types of cyclic batch adsorption processes from each other. Four general desorption methods exist: thermal swing, pressure swing, purge gas stripping and displacement desorption. In thermal swing desorption the adsorbent bed temperature is raised for desorption to take place, while in pressure swing desorption the pressure of the column or adsorbate partial pressure is reduced. Purging can be performed with a non-adsorbed gas or with a gas that includes a component that displaces the product adsorbate from the adsorbent. These methods can also be integrated in various combinations in order to create a hybrid desorption process. (Anderson, 1977, pp. 192–194) A specific variation of pressure swing desorption is vacuum swing desorption, in which desorption takes place at a very low, vacuum-like pressure level (Chao et al., 2021). Adsorption processes are often named based on their respective desorption methods.

For adsorption-based post-combustion carbon capture, the different adsorption processes have their pros and cons. Thermal swing adsorption (TSA) processes are not very strict on the impurity levels of the flue gas as the higher temperature level enables the removal of impurities from adsorbents. However, required higher temperature levels correspond with higher energy requirements and therefore added costs. Pressure swing (PSA) and vacuum swing adsorption (VSA) processes operate at around ambient temperatures and therefore no additional heat needs exist, but a high energy need exists in the form of depressurization and vacuum creation. PSA processes are also more sensitive to impurities. (Chao et al., 2021) Another important consideration is the desorption time. While desorption time in a PSA process can be in the range of seconds to minutes, in TSA the desorption time of bulk component, like carbon dioxide adsorbed from flue gas, can be in the range of hours. (Thomas & Crittenden, 1998e, pp. 127, 131) Only TSA processes will be discussed as it is the process configuration of interest.

A simplified thermal heat and power plant process scheme with post-combustion carbon capture is presented in figure 2.9, where the carbon capture unit is located after the flue gas treatment. Carbon dioxide is one of many combustion products in thermal heat and power plants, along with water vapor and pollutants such as SO_x, NO_x and particulate emissions. The amount of each impurity component in the flue gas depends on the fuel and combustion technology used. As post-combustion carbon capture often requires a rather clean flue gas stream with little impurities, the flue gases need to be purified before the capture process. This is also true for a TSA process even if impurity tolerance is higher than for other adsorption methods.

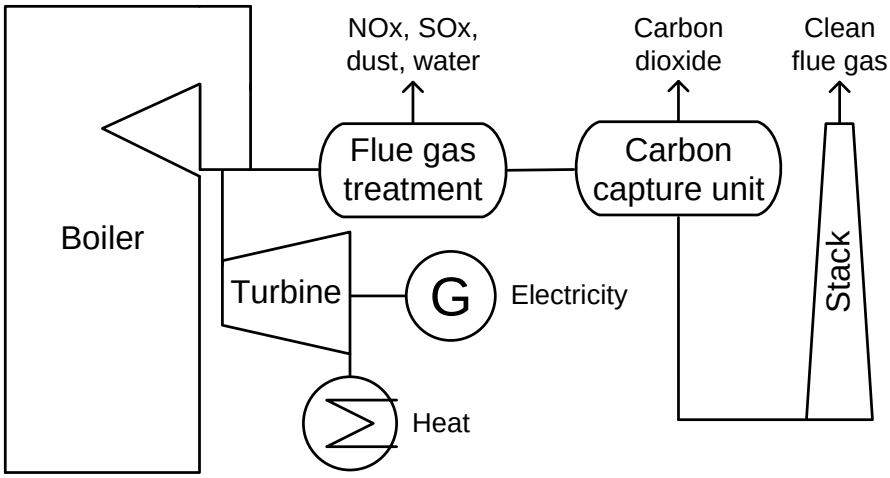

Figure 2.9. *A simplified of a heat and power plant process scheme with an integrated post-combustion carbon capture unit. Process components not in scale.*

In a study by Boumghar et al. (2020), where the effect of impurities was examined, carbon dioxide adsorption was carried out on a gas flow with an inlet composition of 10% CO_2, 250 ppmv SO_2 and 250 ppmv NO with carbon fiber textile as the adsorbent. The results showed that in the short term such impurities have little effect on the adsorption of carbon dioxide, but as the saturation of impurities in the adsorbent had occurred, the carbon dioxide adsorption capacity of the adsorbent decreased up to 25%. (Boumghar et al., 2020) In a separate study by Osaka et al. (2018), which concentrated on the detrimental effect of water in adsorption performance, thermal swing adsorption was conducted with zeolite 13X as the adsorbent on a gas flow with a carbon dioxide concentration of 15%. Results showed that due to the competitive adsorption of water and carbon dioxide, significantly reducing the water content of the flue gas flow is essential in improving carbon dioxide adsorption capacity. (Osaka et al., 2018)

Numerous flue gas treatment methods exist for various impurities that could also affect the carbon capture process. For particulate matter, electrostatic precipitators, mechanical collectors, fabric filters and wet scrubbers can be used. (The Babcock & Wilcox Company, 1972, pp. 2–3) Most common SO_x emission removal methods are based on using calcium compounds in wet scrubbers, namely calcium carbonate ($CaCO_3$) or calcium hydroxide

($Ca(OH)_2$). Calcium compounds can also be injected into the furnace in order to have the undesired compounds already in removable form in the flue gas. (Iisa, 1995, pp. 283–284) One way to control NO_x emissions is by selective non-catalytic reduction (SNCR) or selective catalytic reduction (SCR). In a SNCR process, ammonia (NH_3) is added to hot (around 900 °C) flue gases, resulting in the formation of water and nitrogen gas. In SCR the ammonia is added to cooler (250–500 °C) flue gases which slows down the reaction kinetics and therefore a catalyst is needed. (Kilpinen, 1995, pp. 253–254)

A plain TSA process configuration includes two separate reactor columns of which both act as adsorption and desorption columns. A simplified schematic of a basic TSA configuration is presented in figure 2.10. Both reactors are running simultaneously and continuously but in different steps as one is in the adsorption step and the second in desorption step. As mentioned in section 2.1, the exothermic nature of adsorption leads to the conclusion that lower temperatures increase the adsorption capacity and in turn, increasing the temperature leads to decreasing the amount adsorbed (desorption). This is the basis of a TSA process. Figure 2.11 depicts the isotherm profile of an adsorbate during a simplified TSA process with four distinct steps.

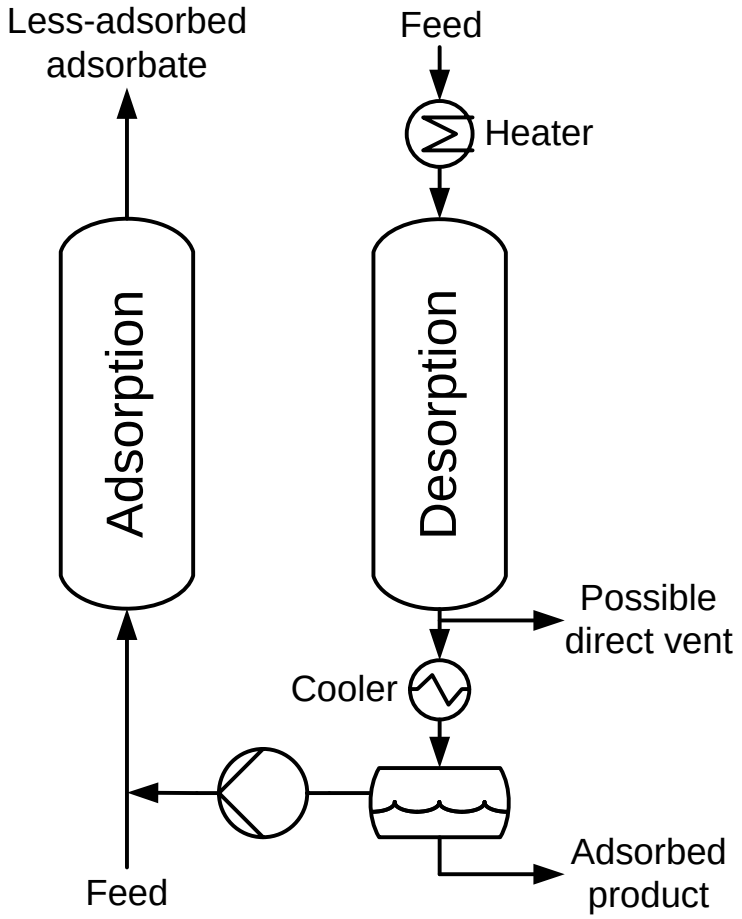

Figure 2.10. *A schematic of a plain temperature swing adsorption process with two separate columns and related process equipment. Adapted from Keller II & Anderson (1987, p. 655).*

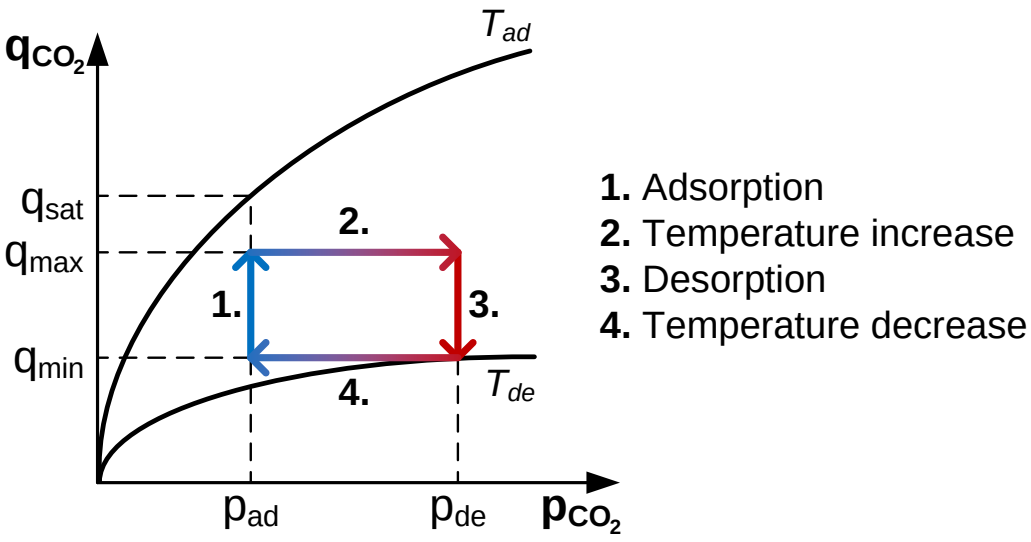

Figure 2.11. *An adsorption isotherm depicting a simplified thermal swing adsorption process cycle, where saturation (equilibrium) adsorbent loading is not reached. Adapted from Jiang et al. (2020).*

In step one, the feed with the desired adsorbate component is fed through the adsorption column. The temperature increase in step two is often achieved with a direct contact by a hot stream of varying kinds, being for example the feed, product or a separate purge gas. A less common way to provide heating is by indirect means with heating elements inside the reactor. As the direct contact stream providing heat for step two also functions as the purge stream in desorption (step three), steps two and three occur simultaneously. The use of product gas as a purge stream leads to higher concentration of the adsorbate in the gas stream. (Thomas & Crittenden, 1998d, p. 131; Sherman, 1991, pp. 547–548)

Rate of desorption has been noted to be limited mostly by the heat transfer rate while the contribution of mass transfer resistance is lesser (Anderson, 1977, p. 183). Therefore, similar regeneration results can be achieved with either a combination of high desorption temperature and low purge gas flow rate or a high flow rate and low temperature (Thomas & Crittenden, 1998d, p. 131). A compromise between the two is usually needed, as higher temperatures lead to considerations on heating costs, choice of materials and the thermal stability of both the adsorbent materials and the fluids involved. On the contrary, higher flow rates lead to larger adsorption columns and therefore higher costs. (Sherman, 1991, pp. 548–549) In general, for recoverable products, higher temperatures are favored as it provides a more convenient way of increasing adsorbate concentration in the outflow (Ruthven, 1984b, p. 343).

As for the temperature decrease in step four, a separate cooling phase is not often utilized. In the adsorption step the thermal wave in the adsorbent bed travels in front of the MTZ. This leads to the MTZ temperature to bed determined only by the feed temperature, not by the bed temperature prior to the adsorption step. By utilizing a feed in a temperature

that is considerably lower than the bed temperature after the regeneration and desorption step, satisfactory cooling is possible to achieve. (Ruthven, 1984b, p. 346; Thomas & Crittenden, 1998d, p. 131)

3. ADSORPTION REACTOR MODELLING

In this chapter, the theoretical background of the modelling tasks is covered. First, the theory of the one-dimensional (1D) modelling conducted via Python is described. This is followed by the description of the two-dimensional (2D) modelling using Ansys Fluent. For both models, a look into prior research is first taken, followed by the theory and equations used.

3.1 Prior studies utilized in one-dimensional model development

The heat and mass transfer models utilized in the one-dimensional model were based on the work by Hwang et al. (1995). In the study Hwang et al. created a non-equilibrium, non-isothermal and non-adiabatic simulation model for a fixed-bed TSA process. The adsorbate gas in the process is carbon dioxide as a bulk component. The process included a number of approximations in order to simplify the simulation. One of the implications was that no other gas components would be adsorbed, only carbon dioxide, leading to a single-component adsorption approximation. A comparison of the simulation data and the experimental data was conducted, with simulation results comparing well with the actual experiments. Activated carbon was used as the adsorbent in the experimental work. The effects of isothermal and adiabatic models were compared with the non-isothermal and non-adiabatic model. In addition, the effects of mass transfer and heat transfer coefficients were studied. The study makes use of heat and mass transfer coefficients as collected parameters and includes the utilization of linear driving force (LDF) model as the mass transfer model. The isotherm model used is an extended, temperature-dependent Langmuir model. (Hwang et al., 1995) The Langmuir model and its variations have been used extensively in modelling and simulation of carbon dioxide adsorption in fixed-bed reactor systems, as exhibited by Shafeeyan et al. (2014).

The isotherm model along with a number of process and adsorbent parameters were gathered from a study by Ntiamoah et al. (2016). They modelled a dual-component TSA process of carbon dioxide and nitrogen from a mixture of the two gas components using Aspen Adsorption modelling software. Experimental data was used to gather isotherm parameters for the modelling procedure, while dual-site Langmuir isotherm was used as the isotherm model for adsorption of both components. The adsorbent material utilized

was zeolite NaUSY. Similarly to Hwang et al. (1995), LDF model was used for mass transfer. Adsorption was conducted at the temperature of 303.15 K, while desorption occured at temperatures of 423.15 K, 473.15 K and 523.15 K, in order to study the effect of temperature on desorption efficiency. Three separate desorption methods were studied: indirect bed heating, hot product gas purge (high carbon dioxide content) and a combination of the two. Adsorption gas composition was 15 mole percentage of carbon dioxide and 85 mole percentage of nitrogen. Heat and mass transfer coefficients were gathered by estimation with the software used. Along that, heats of adsorption for both components were calculated from the experimental data. The resulting carbon dioxide recovery and product purities varied greatly with the desorption temperature, with expected improvement as the desorption temperature was increased. (Ntiamoah et al., 2016)

All the needed process variables and parameters were not readily available in the previously described studies. In particular, fluid-to-solid heat transfer coefficient and particle surface-area-to-volume (SA/V) ratio, which were made use of by Hwang et al. (1995), were not disclosed by Ntiamoah et al. (2016). These values were found in carbon dioxide adsorption studies which were carried out with Aspen Adsorption software. Carbon dioxide adsorption based on a VSA configuration on two zeolites adsorbents (13X and 5A) was studied by Punpee & Phalakornkule (2022). The gas mixtures of interest contained high amounts of carbon dioxide (molar fraction up to 39%). Zeolite 5A properties and parameters were deemed to be closer to the NaUSY zeolite made use of by Ntiamoah et al. and therefore, the fluid-to-solid heat transfer coefficient of 5A was chosen as the best option available. Wilkes & Brown (2022) investigated the viability of a VSA carbon capture process from the flue gas of a open-cycle gas turbine on the zeolite 13X. The flue gas contained a volume fraction of 4.27% of carbon dioxide. The particle SA/V ratio was given in the article, however no specific scientific basis for the value was provided. Both of the studies also employed the dual-site Langmuir isotherm model.

The aforementioned studies formed the basis for the final iteration of the calculation model. However, a variety of studies were examined and used in the initial trial-and-error phase of building the calculation model. Specifically a number of different isotherm models were tested during the development process. These include Langmuir, Toth and Dubinin-Astakhov (D-A) isotherm models. The articles from which the isotherm models and parameters were collected in the testing phase are briefly presented next.

Langmuir isotherm has been used, in addition to Hwang et al. (1995), by many others, including Roy & Moharir (2019). Single- and multi-component adsorption breakthrough and subsequent desorption was modelled using a simple, Matlab-based 1D model. In addition to the straightforward study of adsorption and desorption, the effect of bed length, LDF, flow velocity, maximum adsorbent adsorption capacity and Langmuir isotherm constant were also examined. The results exhibit general adsorption phenomena and give a comprehensive view on the basics of a simple adsorption process. (Roy & Moharir,

2019) Lei at al. (2013) also employed the Langmuir isotherm model in their modelling work of a TSA process for carbon capture from a mixture of carbon dioxide and nitrogen using Comsol Multiphysics software. In contrast to the two aforementioned studies utilizing the Langmuir isotherm model, the model created by Lei et al. is 2D. Only carbon dioxide adsorption was modelled, as the amount of nitrogen adsorbed was deemed to be insignificant compared to carbon dioxide adsorption (around 7% of CO_2 adsorbed). (Lei et al., 2013)

Toth isotherm model was applied by Dantas et al. (2011) in a study of 2D PSA process of carbon capture from flue gas on activated carbon in a fixed-bed reactor. A mathematical model was created based on experimental data and calculated with gPROMS simulation software. The study includes simultaneous adsorption of carbon dioxide and nitrogen with a sophisticated mass transfer coefficient model. (Dantas et al., 2011) Another study, which made use of both the Toth and D-A isotherm models, was conducted by Jribi et al. (2017). Similarly to Dantas et al., Jribi and co-workers modelled a PSA-based carbon capture process on activated carbon. Experimental data was fitted with both Toth and D-A isotherm models and parameters. The LDF model was modified to incorporate a variable mass transfer coefficient for better correlance with the experimental data. (Jribi et al., 2017)

3.2 Governing equations for one-dimensional model and adsorption

As for the mass transfer of adsorption, the general mass transfer equation for an adsorbate component, which does not take into account axial dispersion or velocity variation, is

$$\frac{\partial c_i}{\partial t} + v\frac{\partial c_i}{\partial z} + \frac{1-\varepsilon}{\varepsilon}\rho_s\frac{\partial q_i}{\partial t} = 0, \tag{3.1}$$

where c_i is the concentration of a species in the fluid [$mol_i\, m_f^{-3}$], t is time [s], v is the fluid velocity [$m\, s^{-1}$], z is the axial coordinate [m], ε is the adsorbent material porosity [-], ρ_s is the adsorbent material density [$kg_s\, m^{-3}$] and q_i is the concentration of an adsorbate species on the adsorbent material [$mol_i\, kg_s^{-1}$], also called adsorbent loading. The terms represent, from left to right, the concentration of the adsorbate species in the fluid phase, the convective flow in the reactor and the adsorption rate of a species. (Thomas & Crittenden, 1998e, p. 148–150) The LDF model is used to represent the mass transfer rate between the fluid (adsorbate) and the solid phase (adsorbent) and it is defined as

$$\frac{\partial q_i}{\partial t} = k_i(q_i^* - q_i), \tag{3.2}$$

in which k_i is the mass transfer coefficient of a species [s^{-1}] and q_i^* is amount of a certain

species adsorbed at equilibrium [$mol_i\ kg_s^{-1}$], indicating that when q_i^* equals q_i no more mass transfer (adsorption) of that specific fluid species occurs. (Thomas & Crittenden, 1998e, p. 160) The specific definition of q_i^* depends on the isotherm model used. The dual-site Langmuir isotherm model used by Ntiamoah et al. (2016) is defined as follows:

$$q_i^* = \frac{\lambda_{1,i} e^{\left(\frac{\lambda_{2,i}}{T}\right)} P_i}{1 + \lambda_{3,i} e^{\left(\frac{\lambda_{4,i}}{T}\right)} P_i} + \frac{\lambda_{5,i} e^{\left(\frac{\lambda_{6,i}}{T}\right)} P_i}{1 + \lambda_{7,i} e^{\left(\frac{\lambda_{8,i}}{T}\right)} P_i}, \tag{3.3}$$

in which $\lambda_{1,i}$ through $\lambda_{8,i}$ are experimentally determined isotherm fitting parameters for fluid species i (units for 1 and 5: [$kmol_i\ kg_s^{-1}\ bar^{-1}$]; 2, 4, 6 and 8: [K]; 3 and 7: [bar^{-1}]), T is the temperature [K] and P_i is the partial pressure of the fluid component to be adsorbed [bar]. The definition of T differs between the 1D and 2D models. In the 1D Python model, the temperature is the average between the solid and fluid temperatures. As the 2D Ansys Fluent model does not have a specific separate solid region, the temperature used refers to the fluid temperature.

As for heat transfer, the reactor is approximated to be adiabatic due to insulation. Fluid-to-solid heat transfer and heat generated by adsorption are included in the model. Heat transfer between the fluid and adsorbent is modelled with

$$\varepsilon \rho_f c_{p,f} \frac{\partial T_f}{\partial t} + \varepsilon \rho_g c_{p,f} v \frac{\partial T_f}{\partial z} - h_{f-s} a_p (1 - \varepsilon)(T_s - T_f) = 0, \tag{3.4}$$

in which ρ_f is the fluid density [$kg_f\ m^{-3}$], $c_{p,f}$ is the heat capacity of the fluid [$J\ kg_f^{-1}\ K$], T_f is the fluid temperature [K^{-1}], h_{f-s} is the fluid-to-solid heat transfer coefficient [$W\ m_s^{-2}\ K^{-1}$], a_p is the particle external SA/V ratio [m^{-1}] and T_s is the adsorbent temperature [K]. (Hwang et al., 1995) Similarly, the heat transfer equation in the adsorbent is determined as

$$\rho_p c_{p,s} \frac{\partial T_s}{\partial t} + \rho_s a_p (T_s - T_f) + \rho_p \Delta H_i \frac{\partial q_i}{\partial t} = 0, \tag{3.5}$$

where $c_{p,s}$ is the heat capacity of the adsorbent [$J\ kg_s^{-1}\ K^{-1}$] and ΔH_i is the heat of adsorption of a species [$J\ mol_i^{-1}$]. (Hwang et al., 1995)

3.3 Prior studies utilized in two-dimensional model development

Computational fluid dynamics -based modelling of carbon dioxide TSA processes has not been studied extensively. However, Qasem N. and Ben-Mansour R., with help of co-workers, have conducted a handful of studies on the topic. Studies include experiments and using Ansys Fluent as a modelling tool with integrated user-defined functions (UDF) for successful and accurate adsorption modelling. The adsorption process configurations in the studies include a simple fixed-bed design in either 2D or 3D with the adsorbent material varying, being often a zeolite (namely either MOF-177, Mg-MOF-74 or 13X) or

activated carbon. In many cases, the studied bed geometry is small in size and the flow laminar rather than turbulent.

In two studies that concentrated on the effect of water vapour on the adsorption process, simulating wet flue gas, a dehydration process before adsorption was recommended. In the earlier study, Ben-Mansour et al. (2018) simulated an adsorption process using Mg-MOF-74 as an adsorbent on dry and humid CO_2-N_2 mixtures in ambient conditions. The simulation data was validated against experimental data results from literature and experiments by the authors. In the later study by Qasem & Ben-Mansour (2018a), similar simulations were conducted using 13X and Mg-MOF-74 as adsorbents and the results were validated against experimental data. Both studies concluded that a moisture content above 3% noticeably decreases the adsorption capacity of Mg-MOF-74, while the adsorption capacity of 13X was not affected as significantly. As moisture is not included in the calculations of this thesis, the effect does not have to be taken into account. The dual-site Langmuir isotherm was also made use of in the studies in the modelling of adsorption of CO_2 and N_2 on the adsorbent Mg-MOF-74, however, in a different form than the one used by Ntiamoah et al. (2016).

In both aforementioned studies it was also declared that a 2D Ansys Fluent simulation instead of 3D was sufficient enough to get results that compared well with the experimental data. Different 2D reactor geometries in a carbon dioxide TSA process were investigated and studied by Lian et al. (2019). An important parameter in defining the reactor geometry is the length-to-diameter (L/D) ratio. In the article, three separate L/D ratios were studied: 4.375, 11.2 and 17.5 with the amount of adsorbent, surface area, inlet flowrate, inlet gas temperature and operating pressure being the same in each case. Product purity and recovery rates as well as productivity (amount of product recovered per amount of adsorbent in a unit of time) and energy consumption (needed energy per amount of product recovered) were compared in the simulation cases. As a result, the reactor with an L/D ratio of 11.2 performed best in terms of product purity, recovery and productivity in a five cycles long adsorption-desorption process. (Lian et al., 2019)

While the studies by Ben-Mansour et al. (2018) and Qasem & Ben-Mansour (2018a) provide a detailed description of the adsorption models and the results, the specific UDFs for adsorption are not discussed. In a study by Ye et al. (2012), adsorptive storage of hydrogen was modelled using Fluent software with implemented UDFs, which are described in the article. The D-A isotherm was employed for the adsorption modelling. The attained simulation data showed good agreement with the experimental data.

Although above studies, along with the isotherm model presented in sections 3.1 and 3.2, formed the basis of the simulations conducted with Ansys Fluent, a number of other studies were inspected in order to gain insights on the modelling of the process. These studies will be presented briefly next.

Another study by Ben-Mansour et al. (2017) made use of activated carbon and MOF-177 as adsorbent materials in a 2D transient simulation of the adsorption of carbon dioxide from CO_2-N_2 and CO_2-H_2 mixtures. The processes included PSA as well as high temperature-low pressure and low temperature-high pressure conditions. The results compared well with data obtained from experiments. A five-step VSA process utilizing Mg-MOF-74 as an adsorbent was studied by Qasem & Ben-Mansour (2018b). 2D and 3D simulations were conducted with 2D being once again comprehensive enough for the results to successfully match the experimental data. Operating pressure in the process steps varied between 2–130 kPa and the inlet temperature was 323 K. Good adsorption results were gathered from the simulations with enhanced adsorption parameters compared to those found in literature.

In addition, more specific process parameters in physical adsorption processes have been studied. Results suggest that many of the options available improve the adsorption potential of the process. Ben-Mansour et al. (2020) studied the thermal design variations and its effects on the adsorption capacity of a system. The variations included different bed aspect ratios (keeping reactor volume as a constant), water as a coolant and including heat transfer fins in the adsorption bed. In another study by Qasem & Ben-Mansour (2022) the geometry of the adsorption bed was varied in order to determine the best geometry in terms of adsorption process efficiency. Circular, square and triangular cross-sectional beds were studied. All in all, the conclusion was that a square bed is the optimal choice in terms of pumping power and CO_2 adsorption capacity. In both of these studies Mg-MOF-74 was modelled as the adsorbent.

3.4 Governing equations for two-dimensional model

Porous media model was used to model the adsorbent and flow within the adsorbent bed in the Ansys Fluent software. The mass conservation equation for porous media using physical velocity formulation is expressed as

$$\frac{\partial(\varepsilon\rho_f)}{\partial t} + \nabla \cdot (\varepsilon\rho_f\vec{v}) = S_m, \tag{3.6}$$

in which $\vec{v}$ is the overall velocity vector [m s^{-1}] and S_m is the user-defined mass source [kg m^{-3} s^{-1}] (ANSYS, Inc., 2022b, p. 3; ANSYS, Inc., 2022c, p. 1242). The velocity formulation in the porous medial model was set out to be the physical velocity model, which is defined as

$$\vec{v}_{physical} = \frac{\vec{v}_{superficial}}{\varepsilon} = \vec{v}, \tag{3.7}$$

where $\vec{v}_{physical}$ is the physical velocity [m s^{-1}] which takes into account the porous media and $\vec{v}_{superficial}$ is the velocity [m s^{-1}] determined strictly by the volumetric flow rate, hence the term superficial. The latter does not factor in the porous media and thus does not

model the increase in the velocity due to the porosity, which may lead to inaccurate results (ANSYS, Inc., 2022c, pp. 1240–1241). S_m in equation 3.9, in the context of adsorption, is defined as

$$S_m = -(1-\varepsilon)\sum_i M_i \frac{\partial q_i}{\partial t}, \tag{3.8}$$

in which M_i is the molar mass of a fluid component species [kg mol^{-1}] (Qasem & Ben-Mansour, 2018a). The general momentum conservation equation is defined as

$$\frac{\partial}{\partial t}(\rho_f \vec{v}) + \nabla \cdot (\rho_f \vec{v}\vec{v}) = -\nabla p + \nabla \cdot (\bar{\bar{\tau}}) + \rho_f \vec{g} + \vec{F}, \tag{3.9}$$

where p is the pressure [Pa], $\bar{\bar{\tau}}$ is the stress tensor [Pa], term $\rho_f \vec{g}$ represents the gravitational body force, with $\vec{g}$ being the gravitational acceleration [m s^{-2}], and $\vec{F}$ represents the external body forces [N]. (ANSYS, Inc., 2022b, p. 3) $\vec{F}$ also includes the source term for porous media, often represented as S_n (for the n:th momentum equation of either x, y or z) which, for a simple homogenous porous media, is expressed as

$$S_n = -\left(\frac{\mu}{\alpha} v_n + C_2 \frac{1}{2}\rho |v| v_n\right), \tag{3.10}$$

where μ is the dynamic viscosity of the fluid [Pa s], α is the permeability factor of the porous media [m^2], C_2 is the inertial resistance factor [m^{-1}] and $|v|$ is the magnitude of the velocity [m s^{-1}] (ANSYS, Inc., 2022c, p. 1237). For porous media that represents the conditions of a packed bed, components α and C_2 are defined in Ansys Fluent as

$$\alpha = \frac{d_p^2}{150}\frac{\varepsilon^3}{(1-\varepsilon)^2} \tag{3.11}$$

and

$$C_2 = \frac{3.5}{d_p}\frac{(1-\varepsilon)}{\varepsilon^3}, \tag{3.12}$$

where, in both, d_p is the adsorbent particle diameter [m] (ANSYS, Inc., 2022c, p. 1253). Thermal equilibrium model was chosen to represent the heat transfer between the fluid and the solid in the porous zone, as the heat transfer is expected to be very rapid between the two media. The general energy equation in porous media zone for the thermal equilibrium model in Ansys Fluent (ANSYS, Inc., 2022c) is as follows

$$\begin{aligned}\frac{\partial}{\partial t}(\varepsilon\rho_f E_f + (1-\varepsilon)\rho_s E_s) + \nabla \cdot (\vec{v}(\rho_f E_f + p)) = \\ \nabla \cdot \left[k_{eff}\nabla T - \left(\sum_i h_i J_i\right) + (\bar{\tau} \cdot \vec{v})\right] + S_e,\end{aligned} \tag{3.13}$$

where E_f is the total energy of the fluid [J], E_s is the total energy of the solid [J], k_{eff} is the effective thermal conductivity [W m^{-1} K^{-1}], h_i the enthalpy of a species [J kg^{-1}], J_i is the

mass flux of a species [kg m^{-2} s^{-1}] and S_e is the adsorption energy source term [W m^{-3}]. (ANSYS, Inc., 2022c, p. 1239; Qasem & Ben-Mansour, 2018a). k_{eff} is defined as the volume average of the conductivities of the fluid and the solid in Ansys Fluent as

$$k_{eff} = \varepsilon k_f + (1 - \varepsilon) k_s, \tag{3.14}$$

in which k_f is the fluid phase thermal conductivity [W m^{-1} K^{-1}] and k_s is the solid phase thermal conductivity [W m^{-1} K^{-1}], respectively. In equation 3.13, S_e is the energy source term of adsorption [W m^{-3}], which is defined as

$$S_e = (1 - \varepsilon) \rho_s \sum_i \Delta H_i \frac{\partial q_i}{\partial t}, \tag{3.15}$$

which indicates the release of heat when adsorption occurs. (Qasem & Ben-Mansour, 2018a).

4. MATERIALS AND METHODS

This chapters contains the materials and methods of the thesis process. First, the general research strategy is covered. Following that, a closer inspection of the modelling procedure is taken, with a detailed description of the model building processes. In addition, the general parameters used in the modelling work are presented. Finally, a look into the result comparison and analysis procedure is taken.

4.1 Research strategy

The workflow of this thesis can be divided into three separate parts: literature review, modelling procedure and results analysis, which are presented in figure 4.1. Initial literature review concentrated on the basic theory of adsorption and adsorption processes, especially in the context of carbon capture. The literature review strategy is presented in figure 4.2. The main goal of the literature review was to gain information regarding the process to be modeled and the most important process evaluation indicators in order to successfully build and analyze the models and the gained calculation results. This included going through prior studies in the field of thermal swing adsorption carbon capture modelling, in order to gain general knowledge on the modelling procedure and to obtain potential models and process variables for the modelling work. The literature review provides an answer to the first research question while also setting the research task of building the models.

Modelling procedure, presented in figure 4.3, focuses on constructing of the 1D Python and the 2D Ansys Fluent calculation models, conducting calculations and gathering data. The dual-site Langmuir isotherm model (equation 3.3) parameters along with heats of adsorption and mass transfer coefficients that were used in both models are presented in table 4.1. Other specific modelling parameters are presented in table 4.2. A special aspect of the Ansys Fluent model is the inclusion of UDFs in order to model adsorption and desorption. The calculation models will be further described in detail in the following section, providing a comprehensive answer to the research task of building the models. Once the models were constructed and debugging was carried through successfully, the calculations were performed and essential data was gathered based on the process indicators identified in the literature review.

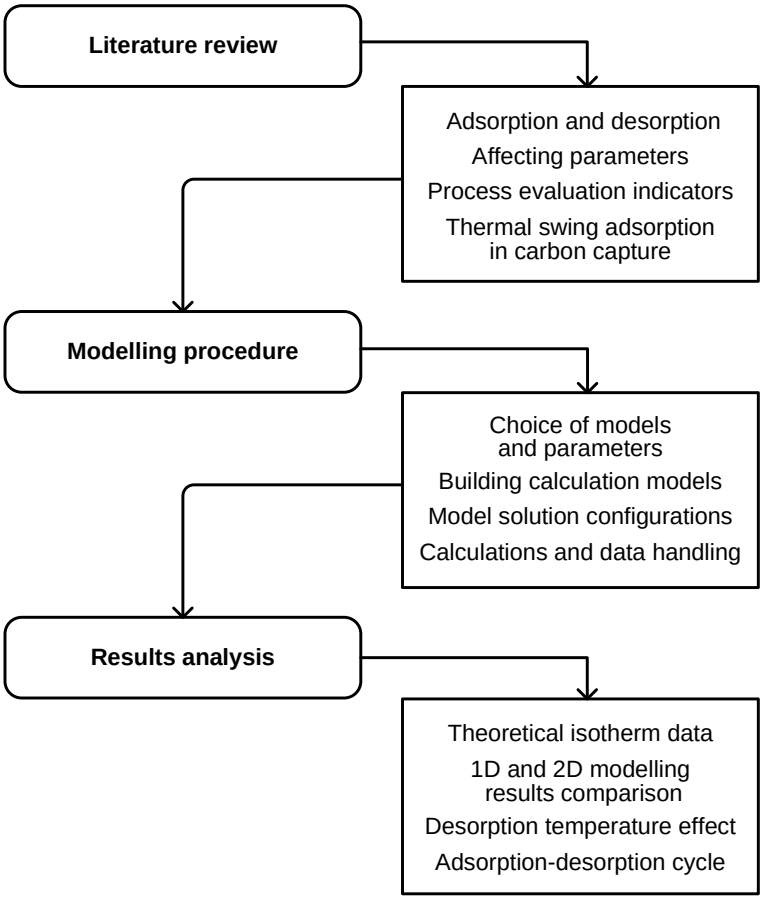

Figure 4.1. *The research strategy divided into three separate steps with main contents of each step described in short.*

Table 4.1. *Dual-site Langmuir isotherm parameters, heats of adsorption and mass transfer coefficients for each adsorbate component. (Ntiamoah et al., 2016)*

Parameter	Unit	CO_2	N_2
$\lambda_{1,i}$	kmol kg_s^{-1} bar^{-1}	0	4.20e-7
$\lambda_{2,i}$	K	30 001	176
$\lambda_{3,i}$	bar^{-1}	0	0
$\lambda_{4,i}$	K	30 184	2.81489
$\lambda_{5,i}$	kmol kg_s^{-1} bar^{-1}	1.99e-6	6.23e-15
$\lambda_{6,i}$	K	2609.32	3.25178
$\lambda_{7,i}$	bar^{-1}	0.03954	1.47395
$\lambda_{8,i}$	K	932.058	1.19157
ΔH_i	J mol^{-1}	-25 800	-15 500
k_i	s^{-1}	0.5	0.3

Table 4.2. *Process parameters and variables used in the calculation models.*

Parameter	Both models	Python (1D)	Ansys Fluent (2D)
Reactor			
Length [m]	1.12[a]		
Diameter [m]			0.1[a]
Cell count [-]		205	56 000
Adsorbent			
Particle density [kg m^{-3}]	1077.354[b,c]		
Particle diameter [m]			0.002[b,d]
Porosity [-]	0.35[b]		
Heat capacity [J kg^{-1} K^{-1}]	1000[b]		
Fluid-to-solid heat transfer coefficient [W m^{-2} K^{-1}]		12[e]	
Particle surface-area-to-volume ratio [m^{-1}]		3000[f]	
Thermal conductivity [W m^{-1} K^{-1}]			0.3[g]
Process variables			
Adsorption inlet gas mole fractions [-]	CO_2: 0.12, N_2: 0.88		
Desorption inlet gas mole fractions [-]	CO_2: 0.88, N_2: 0.12		
Initial reactor temperature [K]	298		
Adsorption temperature [K]	283		
Desorption temperature [K]	373, 423, 523		
Inlet flow velocity [m s^{-1}]		0.42[b]	0.147[h]
Operating pressure [Pa]	101 325		
Time settings			
Process time [min]	90[i]		
Adsorption time step size [s]		0.0075	0.0050
Desorption time step size [s]		0.0075	0.0025

[a]L/D ratio from Lian et al. (2019); [b]Ntiamoah et al. (2016); [c]Calculated using porosity value; [d]Used to calculate porous media resistance parameters (equations 3.11 and 3.12); [e]Punpee & Phalakornkule (2022); [f]Wilkes & Brown (2022); [g]Qasem & Ben-Mansour (2018a); [h]Superficial velocity value, physical velocity value of 0.42 m s^{-1} calculated with equation 3.7; [i]45 minutes of adsorption, followed by 45 minutes of desorption.

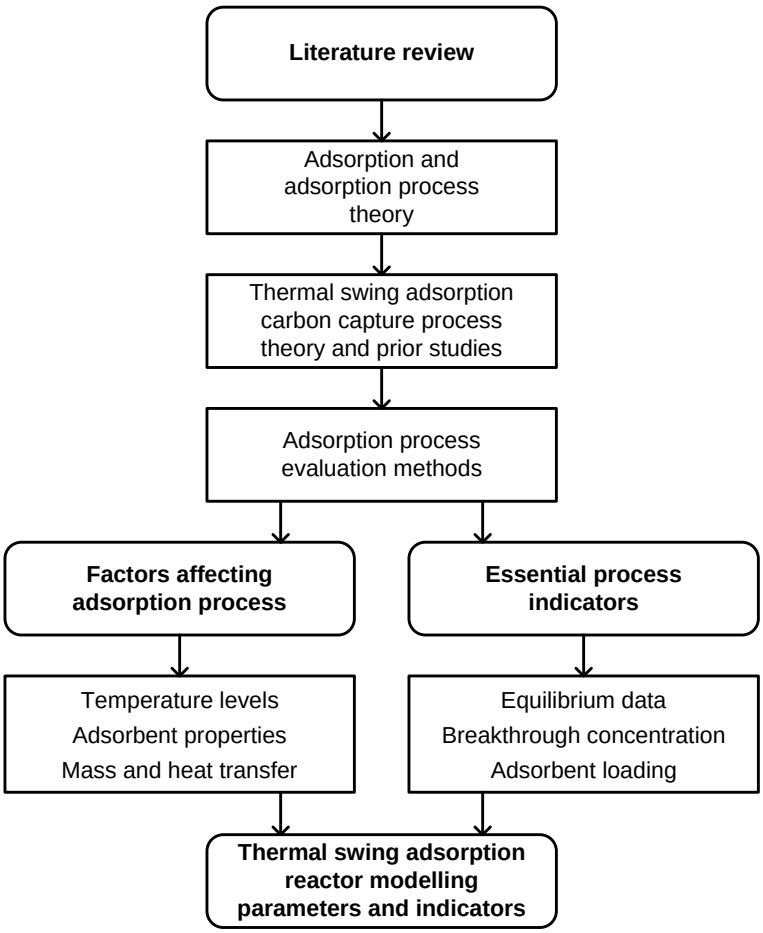

Figure 4.2. *The literature review steps.*

Finally, the results of the two models are compared to each other and a comparison to theoretical isotherm data is also conducted. Since the desorption temperature has been identified as a crucial factor in adsorption process design, the results of the desorption processes at the selected temperatures are further compared and analyzed. The weaknesses and potential areas of improvement in the models encountered during the modelling process are also examined. Therefore, research question three is answered in the results and analysis chapter, while an answer to the research question four is given in the final concluding chapter.

4.2 One-dimensional model construction and formulation

Initial model construction began with intensive studying of prior studies, isotherm models and related heat and mass transfer models. The heat and mass transfer models and equations utilized by Hwang et al. (1995) (presented in section 3.2) were chosen for the calculation model. The isotherm model selection was not as straightforward. Adsorption model building began with studying a simple single-component adsorption process using the Langmuir isotherm model. The study by Hwang et al. (1995) and the isotherm model and parameters included in the study were examined in order to achieve a general idea

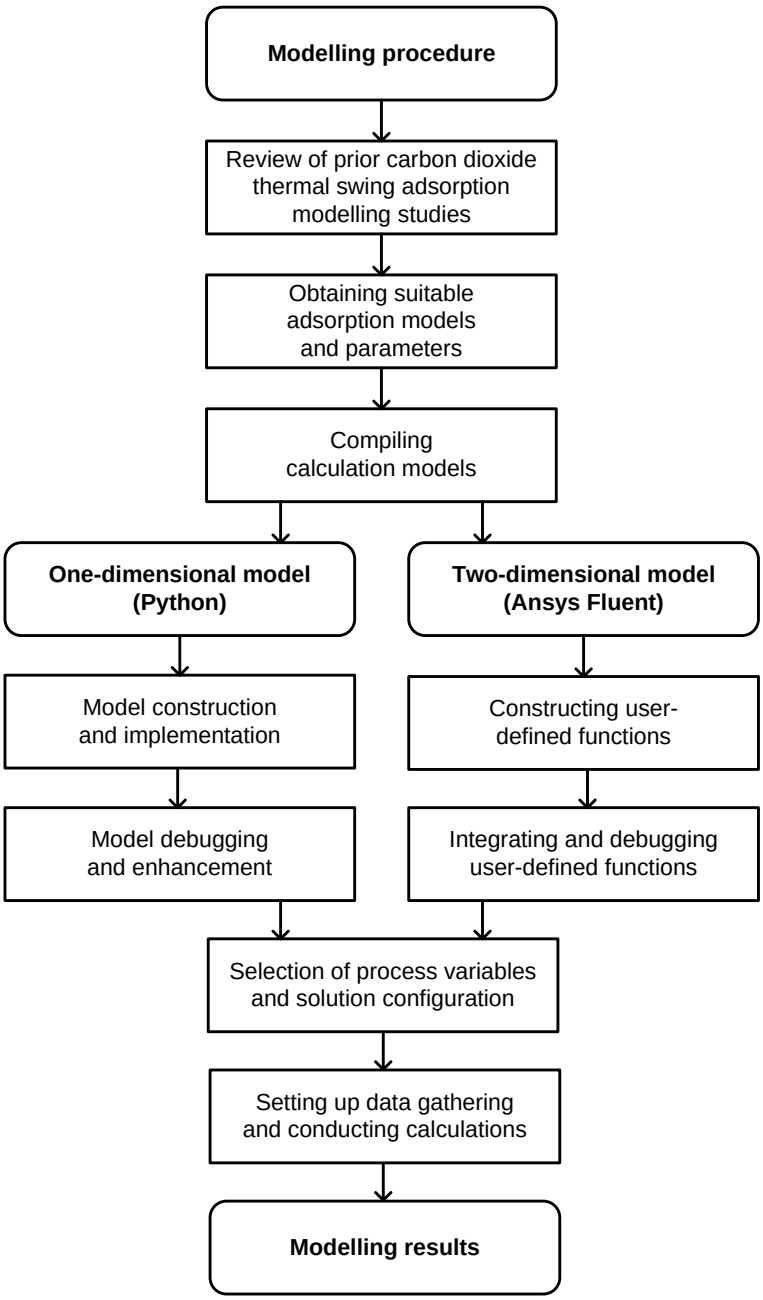

Figure 4.3. *The modelling procedure steps.*

on how adsorption and desorption processes operate. Simultaneously, the Matlab-based adsorption model presented by Roy & Moharir (2019) served as a basis for building the initial code for the adsorption process. Additionally, the isotherm model parameters provided by Lei et al. (2013) were implemented in the adsorption reactor model.

Once a basic understanding of the phenomena in the adsorption and desorption in a simple reactor was gained, the process of selecting a multi-component isotherm model was initiated. The main goal was to find a suitable isotherm model to incorporate at least the adsorption of carbon dioxide and nitrogen. Adsorption of water was not seen as a critical part of the modelling procedure and due to the very limited amount of studies on

the adsorption of all three components, the scope was quickly set on only carbon dioxide and nitrogen. Models for other impurities were not found either. While the final choice was the dual-site Langmuir isotherm with parameters provided by Ntiamoah et al. (2016), other models and parameters were tested and considered. The model development process included a significant amount of trial-and-error. Two separate Toth isotherm models and parameters provided by Dantas et al. (2011) and Jribi et al. (2017) along with D-A isotherm model and related parameters also given out in the same study by Jribi et al. were initially implemented in the adsorption model.

The adsorption process configuration by Ntiamoah et al. (2016) included a favorable desorption configuration using hot, carbon dioxide rich product gas as the purge gas. Alongside that, the abudant availability of related process parameters in the study and the successful initial modelling results were among the major reasons for the final selection of the isotherm model used. The dual-site Langmuir model with parameters provided by Qasem & Ben-Mansour (2018a) was also considered as an option, but as Qasem & Ben-Mansour had already conducted a number of studies using Ansys Fluent and the isotherm model would be used in both calculation models, the task of repetition did not feel suitable. Instead, as Ntiamoah et al. (2016) had used Aspen Adsorption as the modelling software, implementing the isotherm model with its parameters from another software fit the scope of the modelling better.

The construction of the calculation model included discretizing mass and heat transfer partial differential equations (PDE) 3.1, 3.4 and 3.5 into ordinary differential equations (ODE) using finite-difference method for the purpose of solving the equations using Python. SciPy computing library (Virtanen et al., 2020) was used to attain a convenient ODE solver for the modelling case. From the library, `scipy.integrate.solve_ivp` (The SciPy Community, 2023) was chosen as the solver model with backward differentiation formula as the solver method, while CoolProp library (Bell et al., 2014) was used to gather physical properties of fluids which were not deemed to be constant. Namely, heat capacities and densities of fluid properties were calculated as a function of temperature and pressure on each time step of the simulation.

Other parameters (presented in tables 4.1 and 4.2) were kept as constants. The choice of neglecting velocity and pressure gradients in the 1D reactor model was done for the sake of simplicity, as the objective of the 1D model was to be as simple as possible while still possessing required modelling capabilities. The gradients and 2D phenomena were left to be solved in the 2D model using Ansys Fluent.

As for calculations, the cell count of the 1D model was kept reasonably low. This was done to ensure short simulation timescales and to keep the 1D model quick to operate and test. Time step size did not have a considerable effect on the simulation time, whereas higher cell counts lengthened the simulation times considerably. In order to successfully perform

the calculations, the calculation domain needed to be initialized with a trace amount of either fluid component (carbon dioxide or nitrogen), equaling to less than 0.01% of the inlet concentration of either component. This can be considered as a non-factor in regards to the actual calculations and the results.

4.3 User-defined functions for adsorption in two-dimensional model

As Ansys Fluent does not possess capabilities to model adsorption and desorption with the built-in models, the need for externally defined UDFs was recognized. UDFs are written and defined in programming language `C` or `C++` and implemented within the Ansys Fluent software. The use of UDFs can include user-defined scalars (UDS) and user-defined memory slots (UDM). With a UDS the user can include personalized scalars which for the transport equation is subsequently solved (ANSYS, Inc., 2022c, p. 1629). UDMs can be used to store variable values from, for example, the solved UDFs. (ANSYS, Inc., 2022a, p. 360)

All UDFs used in Ansys Fluent are defined using built-in `DEFINE`-macros. A large variety of different types of UDF-macros exist to satisfy a plethora of modelling needs. These macros are described in detail in the Ansys Fluent Customization Manual (2022a). The macros used in the UDFs constructed for the adsorption modelling process are by type `DEFINE_ADJUST` and `DEFINE_SOURCE`. `DEFINE_ADJUST` is a versatile, multi-purpose macro for altering and customizing variables which are not given as arguments. `DEFINE_SOURCE` can be utilized to define source terms for the transport equations solved within the calculations. (ANSYS, Inc., 2022a, pp. 20, 147)

In this modelling work, equations 3.2 and 3.3, including the prequisite calculations in defining fluid component partial pressures, were handled inside the `DEFINE_ADJUST`-macro. Alongside that, the values of the adsorption mass and energy source terms (equations 3.8 and 3.15) were calculated within the said macro. However, the final source term values were handled and passed on in Ansys Fluent using the `DEFINE_SOURCE`-macro type. A total of 12 variables were stored in UDMs for the purpose of executing the calculations within the UDFs and gathering data from the simulations in the software. The work by Ye et al. (2012) and Qasem & Ben-Mansour (2018a), presented in section 3.3, was employed as a strong basis in constructing the UDFs. Just as with the 1D model, building and debugging the UDFs required a substantial amount of trial-and-error.

4.4 Reactor model and solution configuration in two-dimensional model

The 2D geometry of the reactor was created using SpaceClaim included in the Ansys Workbench application, with the meshing done within the same application using Ansys Meshing. The 2D reactor geometry is a simple rectangle with the length of 1.12 meters and diameter of 0.05 meters. The set 0.05 meter diameter in the geometry and mesh effectively doubles up to 0.10 meters with the use of the 2D axisymmetrical geometry configuration in Ansys Fluent, which is considered to be the actual diameter of the reactor. This L/D ratio was chosen based on the work by Lian et al. (2019). The reactor geometry is depicted in figure 4.4, with data collection points along the reactor length marked (further described in section 4.5). A mesh independence study was performed for a portion of the adsorption process step. The mesh grid was kept rather coarse at 56 000 cells due to computational cost and the ultimate task of creating a working model instead of the most accurate one. Simple square cells with the height and width of 0.1 mm were used throughout the mesh, totaling for a 50 by 1120 cell mesh. Using a significantly higher amount of cells would most likely have increased the accuracy but also the computational cost.

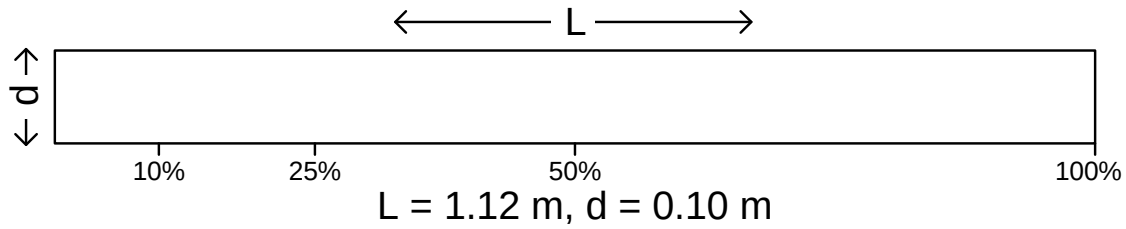

Figure 4.4. *A depiction of the reactor geometry used in Ansys Fluent calculations with the data collection points along the reactor length indicated.*

In the general setup of calculation settings, pressure-based solver was chosen with absolute velocity formulation. Transient time setting was used, as was axisymmetric setting for the 2D space. Gravity was included with 9.81 $\mathrm{m\,s^{-2}}$ as the value opposite to the direction of the flow, simulating a vertical flow upwards. As for the model setup, the energy equation was set on due to temperature effects. Standard k-ε was chosen as the viscous model while species transport was set on. The fluid materials used were carbon dioxide, nitrogen, helium. The properties of a pre-set solid material were edited to represent the adsorbent material. The material property settings are described in table 4.3. Helium properties were left as default, along with molecular weights and L-J parameters.

From the cell zone conditions, porous zone was chosen to represent the adsorbent material. Along that, source terms were included to incorporate the mass and energy source terms of adsorbate species. Viscous resistance and inertial resistance values were calculated with equations 3.11 and 3.12. Thermal equilibrium model was used with solid ma-

Table 4.3. *Material property settings (models and values) used in the Ansys Fluent calculations.*

Property	Carbon dioxide	Nitrogen	CO_2-N_2 mixture	Helium	Solid
Density [kg m^{-3}]	incompressible-ideal-gas	incompressible-ideal-gas	incompressible-ideal-gas	0.1625	1077.354
Specific heat [J kg^{-1} K^{-1}]	piecewise-polynomial	piecewise-polynomial	mixing-law	5193	1000
Thermal conductivity [W m^{-1} K^{-1}]	kinetic-theory	kinetic-theory	mass-weighted-mixing-law	0.152	0.3
Viscosity [kg m^{-1} s^{-1}]	kinetic-theory	kinetic-theory	mass-weighted-mixing-law	1.99e-5	-
Mass diffusivity [m^2 s^{-1}]	-	-	kinetic-theory	-	-
Molecular weight [kg kmol^{-1}]	44.00995	28.0134	-	4.0026	-
L-J characteristic length [Å]	3.941	3.621	-	-	-
L-J energy parameter [K]	195.2	97.53	-	-	-

Table 4.4. *Solution methods used in the Ansys Fluent calculations.*

Solution method	Setting
Pressure-velocity coupling	
Scheme	SIMPLE
Flux type	Rhie-Chow: distance-based
Spatial discretization	
Gradient	Least squares cell -based
Pressure	Second-order
Momentum	Second-order upwind
Turbulent kinetic energy	First-order upwind
Turbulent dissipation rate	First-order upwind
Carbon dioxide	Second-order upwind
Nitrogen	Second-order upwind
Energy	Second-order upwind
Transient formulation	First-order upwind

terial properties that were introduced in table 4.3. Boundary conditions were left mostly unaltered, apart from the inlet and outlet temperatures as well as inlet mole fractions. The turbulence specification method for both the inlet and outlet was set as "Intensity and Hydraulic Diameter" with turbulent intensity as the default value of 5% and hydraulic diameter as 0.05 meters.

The solution settings include solution methods, which are presented in table 4.4. These were left unaltered, as were solution control settings. The solution methods are described in detail in Ansys Fluent Theory Guide (2022b). Standard initialization was used as the initialization method, as suggested in the Ansys Fluent User's Guide (2022c), as hybrid initialization disregards the porous media settings. Initialization also included setting the initial reactor temperature at 298 K, as was done in the 1D model. And, similarly to the 1D model, the reactor was initially thought to be filled with an inert gas. Therefore the reactor was initialized with helium, as helium did not participate in the adsorption step of the process. The 2D model exhibited high sensitivity to the time step size, with seemingly reasonable time steps providing no sensible results. The final time step size choice was done with similar reasoning to the grid size - a compromise between computational cost and accuracy.

4.5 Model result comparison and analysis

After collecting the various data from the calculations of both models, a validation of the results was conducted. As the data could not be compared with any experimental data,

information from scientific articles and books were used as material for validation. The results gathered from the calculations indicated that the models can be used to model adsorption and desorption processes, with behaviour similar to many prior studies that were conducted in the field of TSA of carbon dioxide.

After the validity check, a comparison and a subsequent analysis of the results was carried out. Theoretical isotherms for the isotherm model used were plotted to gain knowledge on the theoretical adsorbent loading levels in adsorption and desorption. Some of the vital process parameters recognized in the literature review were adsorbate concentration (related to breakthrough curves), temperature and adsorbent loading. The results include plots of these parameters as a function of time during the processes. Contours from Ansys Fluent are also presented. Adsorption and desorption steps of the process are separated in the context of result presentation and analysis. This is due to the very different nature of adsorption and desorption, along with the fact that three separate desorption processes with varying temperatures were modelled. The complete adsorption-desorption cycle is addressed when analyzing the mean adsorbent loading of the whole adsorbent bed during the cycle and the achieved adsorbent loading levels are compared to the theoretical values.

As results were gathered from a number of locations along the length of the reactors, comparisons are also made between these locations during the processes. While the data in the 2D model was gathered from exact coordinates along the length of the reactor, the limitations of the 1D model lead to this not being exactly possible. As data in the 1D model was gathered exactly from the middle points of the calculation cells, the coordinate along the reactor for certain points corresponds to an approximate value of the desired point. The points of reactor and according axial coordinates from which data retrieval was set up, as depicted in figure 4.4, are:

- 10% (2D: 0.112 m, 1D: 0.112 m),
- 25% (2D: 0.28 m, 1D: 0.2814 m),
- 50% (2D: 0.56 m, 1D: 0.56 m) and
- 100% (2D: 1.12 m, 1D: 1.1173 m).

As can be seen, the coordinate differences between the models are in the magnitude of two to three millimeters at most. Therefore, comparing data from such points can be considered to be within reasonable accuracy range. The data from the 1D model was gathered as the value from the calculation cell. In the 2D model the data was set to be collected as the area-weighted average, taking the average value along the axial coordinate in the reactor from the whole diameter of the reactor.

Another difference between the models is in the definition of temperature, as mentioned in section 3.2 when describing the dual-site Langmuir isotherm model equation 3.3. The

temperature data from the 1D model refers to the average temperature between the fluid and adsorbent. In the 2D model, no specific solid region temperature was determined as the used thermal equilibrium model considers the temperature level to be of the fluid temperature. These were the definitions of temperature used in equation 3.3 in the models. Therefore, temperature-related comparisons are made based on the selected definitions of temperature.

5. RESULTS AND ANALYSIS

The results of the calculations are presented in this chapter. First, the mesh independence study results are briefly demonstrated. After that, the theoretical isotherm data from the isotherm model used is presented. Following that, the results of adsorption and desorption from both calculation models are showcased and compared. Finally, the adsorption-desorption cycle is analyzed briefly.

5.1 Two-dimensional model mesh independence study

A mesh independence study was conducted for five separate mesh element numbers in the 2D model, ranging from 24 651 to 100 027 cells. The adsorption step was simulated for ten minutes for each mesh size case. The results of the mesh independence study are presented in figure 5.1.

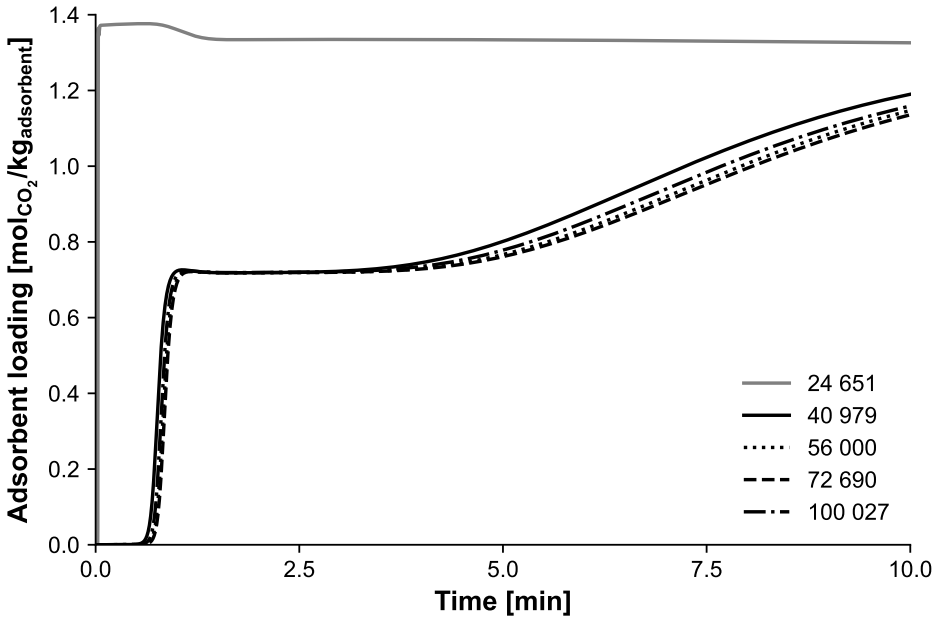

Figure 5.1. *Adsorbent loading of carbon dioxide at 10% of reactor length in the first 10 minutes of adsorption process. Five separate amounts of mesh cells were inspected for the means of a mesh independence study. Amount of cells for each case are indicated in the legend.*

It is evident that when the mesh is too coarse, the results are not reasonable at all, as can

be seen from the adsorbent loading profile in the case of 24 651 cells. With increased cell count, the variation in the results is reduced significantly. In the four other cases, only the cell count of 40 979 varies from the others noticeably. Cell counts between 56 000 to 100 027 show very little variation in the loading profile. A mesh with 56 000 was selected for the calculations due to the results having good agreement with the higher cell counts while reducing the computational cost and calculation times.

5.2 Theoretical isotherm data

The isotherms of the dual-site Langmuir model (equation 3.3) with the parameters provided by Ntiamoah et al. (2016) (presented in table 4.1) for both carbon dioxide and nitrogen are presented in figures 5.2 and 5.3. It is worthy to note that often the x-axis of the isotherm has pressure or partial pressure values of an adsorbate. Here on the x-axis is the molar fraction of an adsorbate for clarity. The pressure in the 1D model is a constant at 101 325 Pa while in the 2D model the pressure level was expected to stay within a reasonable range around the operating pressure.

In order to give a good approximation of theoretical values for the maximum adsorbent loading levels in the adsorption and the minimum adsorbent loading levels in desorption, the loading values of interest are indicated in subfigures 5.2b, 5.3a and 5.3b. A comparison of the calculation results with the theoretical values is given in the final section of this chapter. It is worthy to note that if adsorption was conducted at a temperature of 298 K and desorption at a temperature of 373 K, with the chosen adsorption and desorption gas compositions the desorption carbon dioxide adsorbent loading level would almost equal the achieved maximum adsorbent loading of the adsorption step. This is depicted in subfigure 5.2b. And, as mentioned in section 2.4, as adsorption processes are not isothermal, the isotherm projection is more of a representation of the equilibrium state, as will be shown in the coming sections. The isotherms presented here resemble, but do not closely follow, the behavior of isotherm type I, depicted in chapter 2 in figure 2.6.

5.3 Adsorption step

The length of the adsorption step in the adsorption-desorption cycle was limited to 45 minutes. This was done due to substantially long simulation times using Ansys Fluent. With Python the simulation times were reasonable, but for the purpose of comparison, the adsorption time was kept at 45 minutes for both models.

Adsorption breakthrough curves for carbon dioxide and nitrogen for both models are depicted in figure 5.4. Subfigure 5.4a represents the breakthrough curve at 10% of reactor length and subfigure 5.4b at the outlet. On the y-axis of both subfigures is the concentration ratio (component concentration at axial coordinate divided by the inlet concentration).

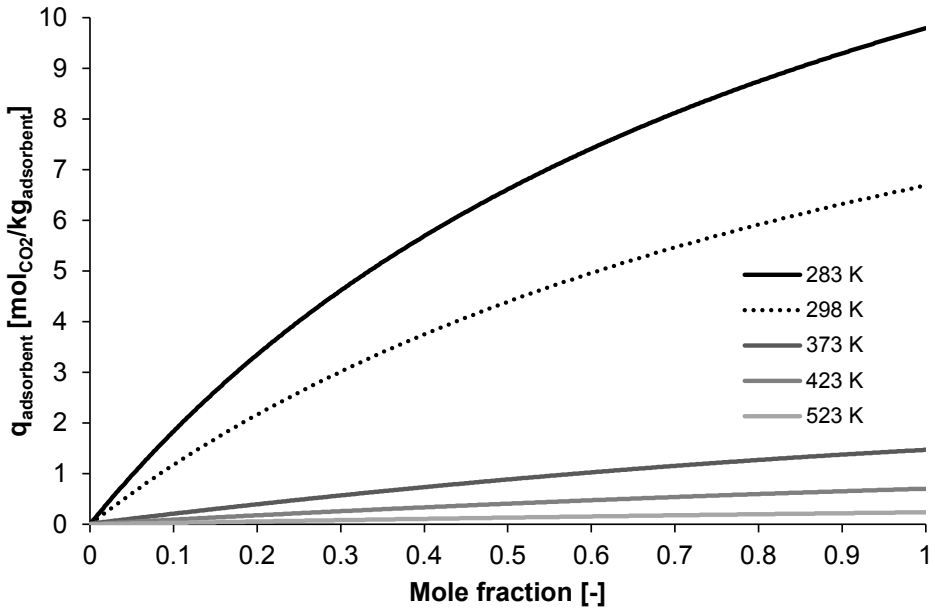

(a) *Carbon dioxide adsorption isotherm at different temperature levels.*

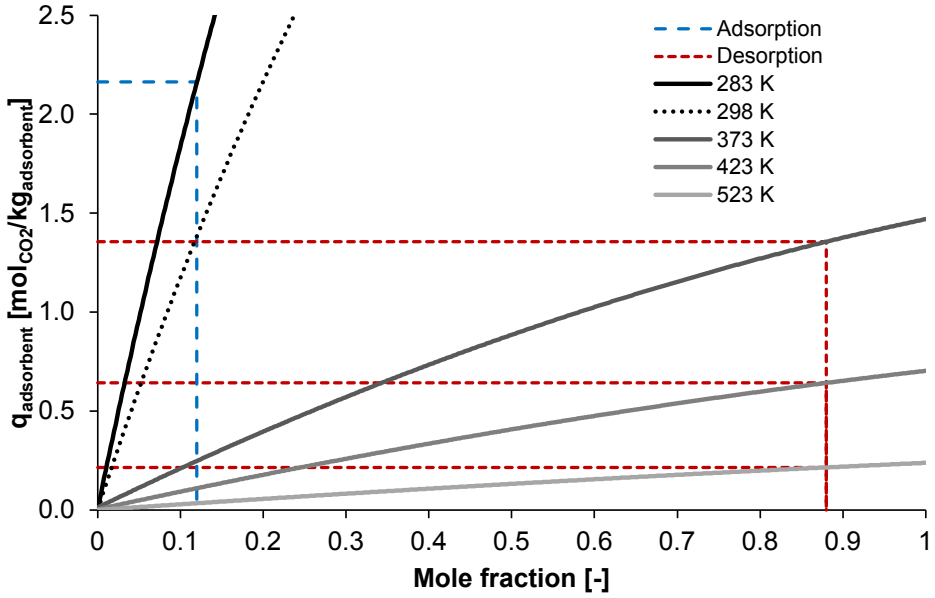

(b) *A closer view of the carbon dioxide adsorption isotherms. Adsorption and desorption mole fractions with according theoretical adsorbent maximum and minimum loading levels are also depicted.*

Figure 5.2. *A depiction of the carbon dioxide isotherm at constant pressure of 101 325 Pa with adsorbate mole fraction on the x-axis, based on the dual-site Langmuir isotherm model and parameters by Ntiamoah et al. (2016) with zeolite NaUSY as the adsorbent. Temperature level of each isotherm is indicated in the legend.*

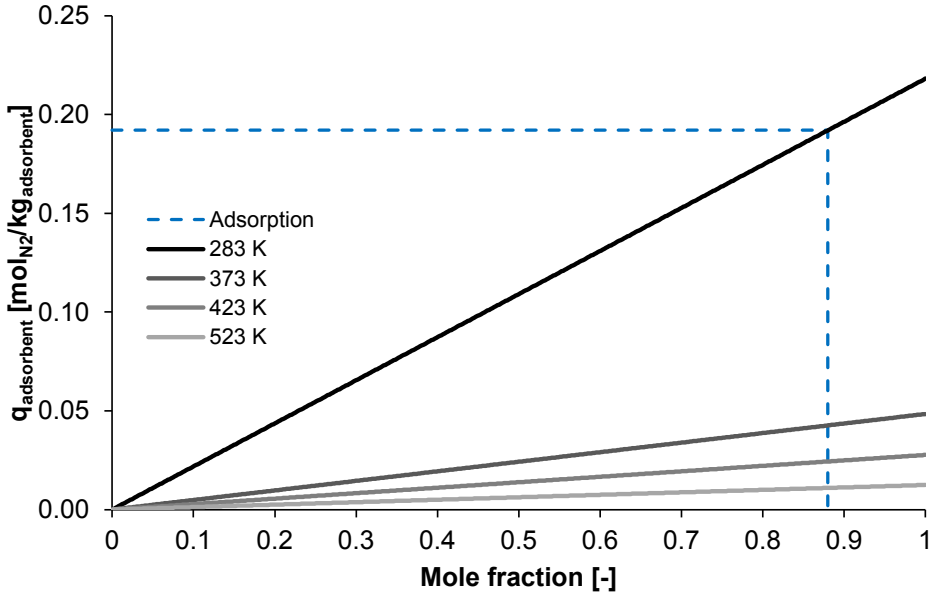

(a) *Nitrogen adsorption isotherm at different temperature levels with adsorption mole fraction and according theoretical maximum adsorbent loading level.*

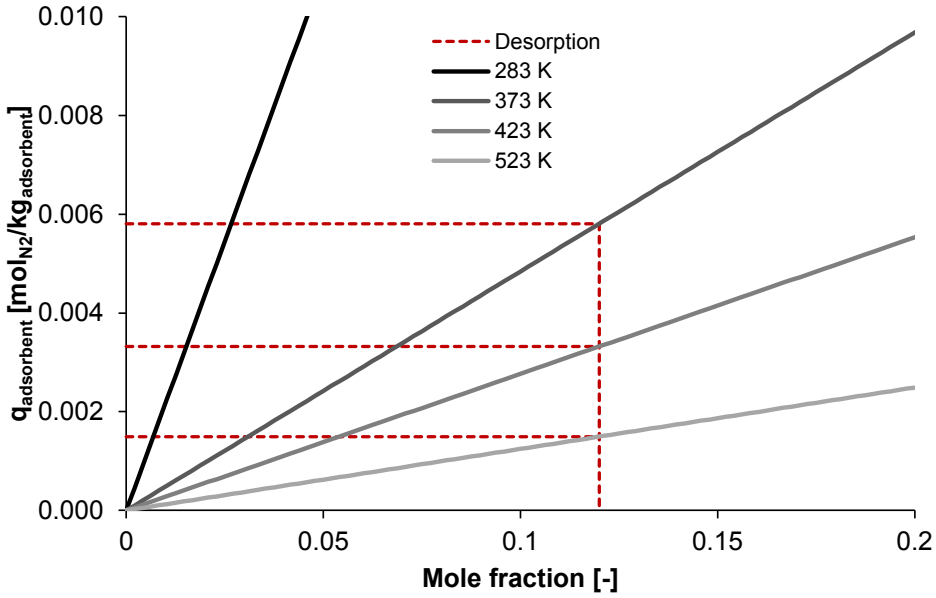

(b) *Nitrogen adsorption isotherm at different temperature levels with desorption mole fraction and according theoretical minimum adsorbent loading levels.*

Figure 5.3. *A depiction of the nitrogen isotherm at constant pressure of 101 325 Pa with adsorbate mole fraction on the x-axis, based on the dual-site Langmuir isotherm model and parameters by Ntiamoah et al. (2016) with zeolite NaUSY as the adsorbent. Temperature level of each isotherm is indicated in the legend.*

Values above one for nitrogen indicate that the bed reaches saturation for nitrogen while adsorption of carbon dioxide continues. In subfigure 5.4a it can be seen that after the initial peak in carbon dioxide concentration ratio, in both models the concentration ratio of carbon dioxide reaches the value of 1.0 after a long period of time. Eventually, both models do reach equilibrium at 10% of reactor length and from that time point on, no more adsorption occurs at that location in the reactor, meaning that the MTZ depicted in subfigure 2.7b has passed that point. The approximate breakthrough times are indicated in the subfigure. On the contrary, no equilibrium is reached at 100% of reactor length in the 45 minutes of adsorption, as shown in subfigure 5.4b. Based on the adsorption process calculations conducted with Python, to reach the equilibrium at the outlet, some five to six hours of process time was needed. The results of the two models presented in figure 5.4 seem fairly similar for both adsorbate components. In general, the trends are similar to the multi-component breakthrough curves presented in figure 2.8. However, the total saturation of both components is reached very slowly, even at 10% of bed length.

The adsorbent loading profiles of carbon dioxide and nitrogen for both models are presented in figure 5.5. Subfigure 5.5a depicts the adsorbent loading of carbon dioxide and subfigure 5.5b depicts the equivalent of nitrogen, respectively. It is demonstrated that both models at all three locations show similar adsorbent loading profiles throughout the 45 minute adsorption process. The most notable differences can be detected for carbon dioxide in subfigure 5.5a at 10% of reactor length. The 2D model plot flunctuates slightly. This can be most likely be accounted for the varying velocity profile near the entrance of the calculation domain. Apart from that, as in the concentration ratio plots in figure 5.4, the plot trends of the two models are similar throughout. General agreement of the models is also noted by the fact that adsorbent equilibrium loading is reached at 10% of reactor length for both models, with adsorbent loading values being in the theoretical value range presented in figures 5.2 and 5.3.

Adsorption step temperature levels are depicted in figure 5.6. Subfigure 5.6a represents the temperature levels of both models at three separate reactor locations. It is evident that the heat release of adsorption causes a temperature increase of around 30 to 35 K from the initial reactor temperature of 298 K. The one-dimensional model temperature peak is slightly higher than in the two-dimensional model, which may be accounted to the definition of temperature in the models. Eventually, the cooler flue gas flow starts to cool down the temperature in the reactor and at 10% of reactor length both models reach the inlet gas flow temperature of 283 K.

Subfigure 5.6b represents the effect of temperature on the adsorbent loading level of both adsorbate components for both models at 10% of reactor length. The adsorbent loading level of carbon dioxide rapidly rises to around 0.7 $\mathrm{mol\,kg^{-1}}$ in both models, which leads to a temperature rise. It is noteworthy that even though the temperature peaks due to adsorption differ between the models, the adsorbent loading level is very similar. The

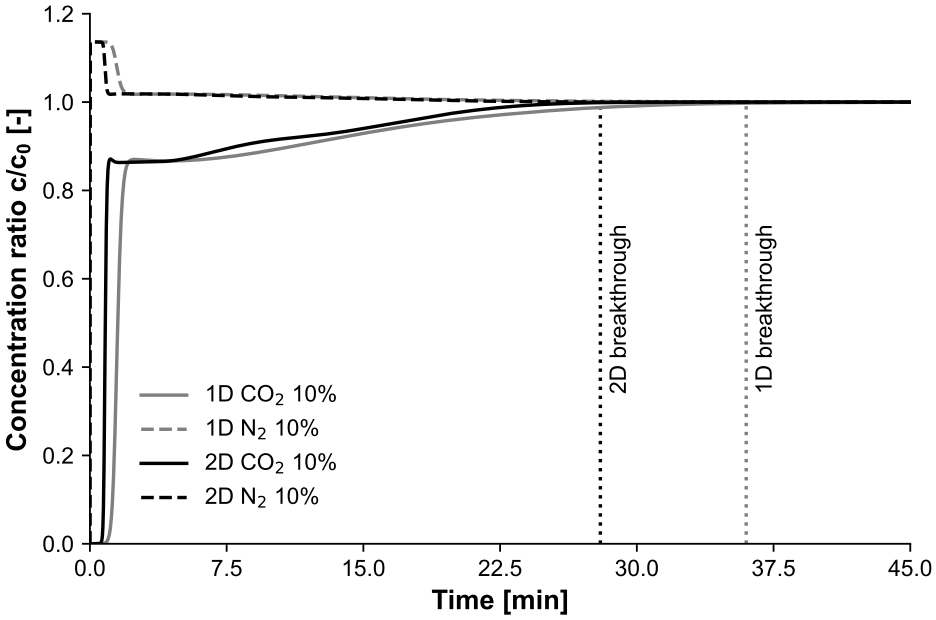

(a) *Breakthrough curve at 10% of reactor length. Initial concentration is reached for nitrogen and carbon dioxide in both models. Approximate breakthrough times for both models are indicated.*

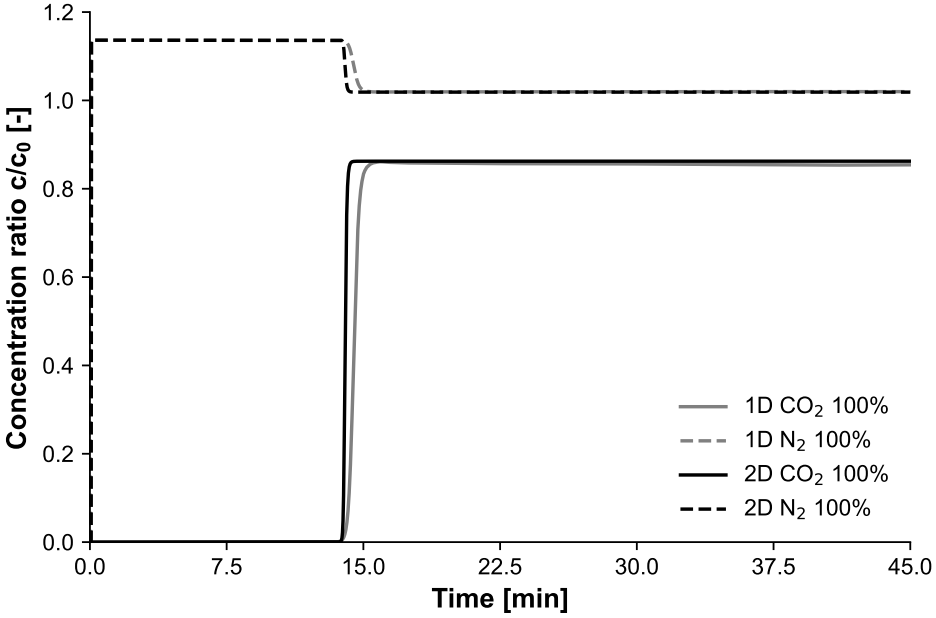

(b) *Breakthrough curves at 100% of reactor length. Initial concentration for carbon dioxide at the outlet is not reached in either model.*

Figure 5.4. *Adsorption breakthrough curve comparison of the one-dimensional and two-dimensional models at two separate locations of the axial length of the reactor (indicated in the legend). On the y-axis c/c_0 is the concentration ratio.*

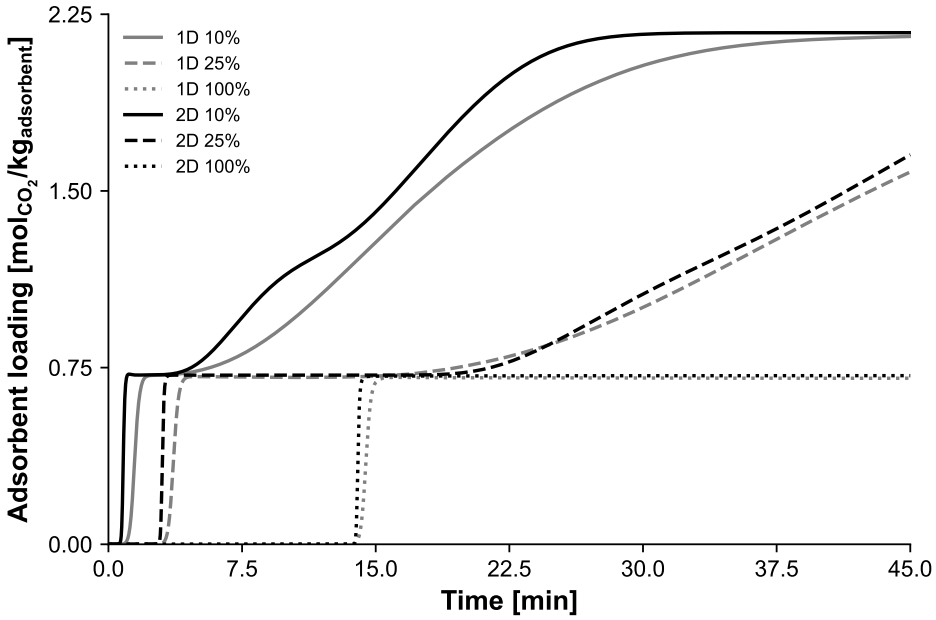

(a) *Adsorbent loading profiles for carbon dioxide.*

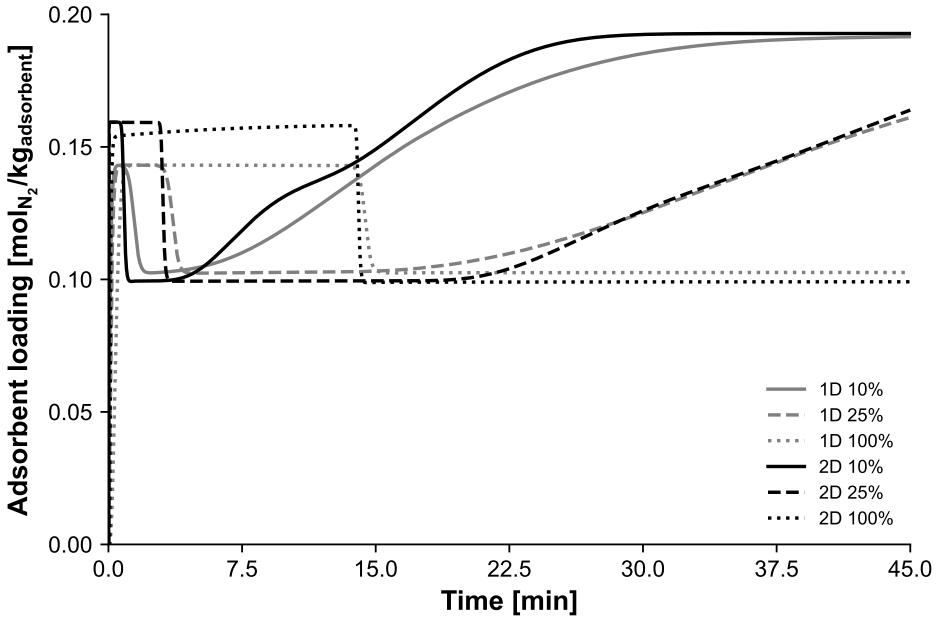

(b) *Adsorbent loading profiles for nitrogen.*

Figure 5.5. *Comparison of one-dimensional and two-dimensional model results of adsorption step adsorbent loading profiles for carbon dioxide and nitrogen at three separate axial locations in the reactor (indicated in the legend).*

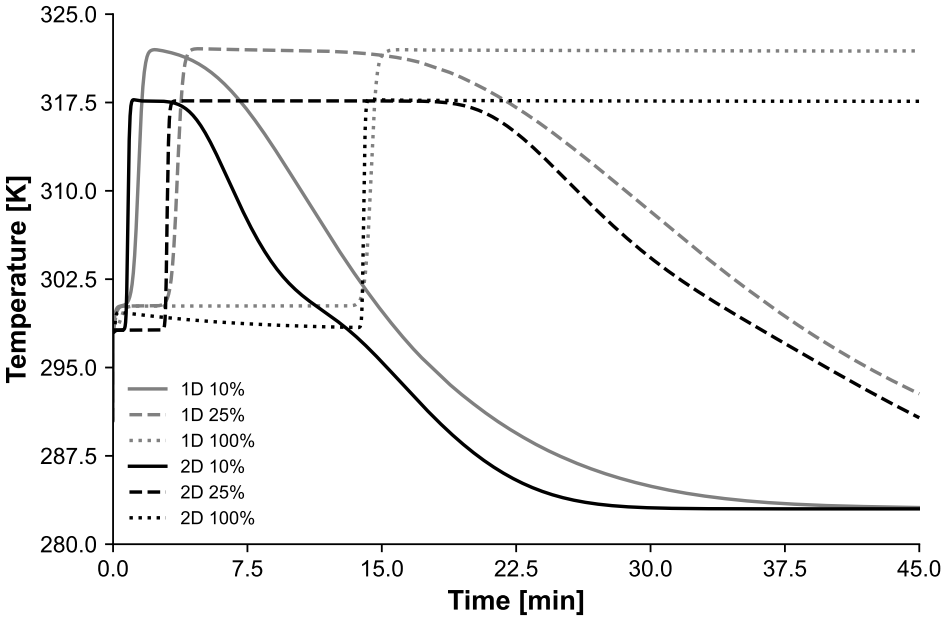

(a) *Temperature level comparison at three separate reactor locations (indicated in the legend).*

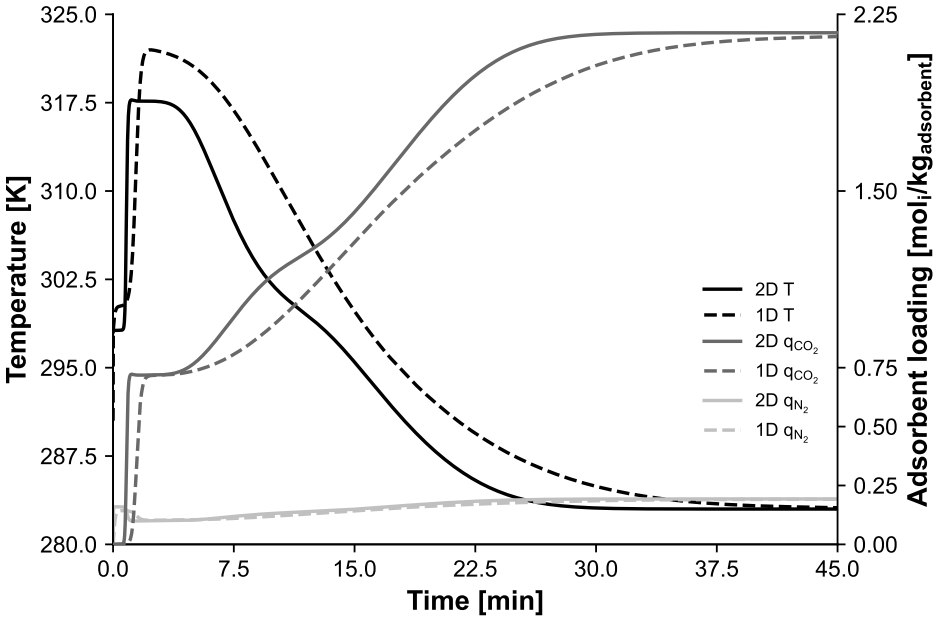

(b) *A plot of temperature and adsorbent loading of components, depicting the effect of temperature on adsorbent loading. The data is gathered at 10% of reactor length.*

Figure 5.6. *Comparison of temperature levels at different reactor locations and depiction of effect of temperature on the adsorption of components during the adsorption step. Results of both models included.*

theoretical values indicate that, at the temperature peak of around 317.5 K, the adsorbent loading in the 2D model should be higher. No clear cause for this phenomenon was discovered. The rising temperature due to the heat of release caused by adsorption initially slows down the adsorption of carbon dioxide. As the cooling effect of the flue gas starts taking place, the temperature inside the reactor stars to decrease. This leads to rising carbon dioxide adsorbent loading until equilibrium loading level is reached. To a lesser extent, a similar effect is seen with the adsorbent loading of nitrogen.

5.4 Desorption step

Similarly to the adsorption step, the desorption process step length was also limited to 45 minutes. This was due to even smaller time step in the 2D model compared to the adsorption step with three separate desorption processes to be modelled, further increasing the total calculation time.

Figure 5.7 depicts the adsorbent loading profiles during desorption. In subfigures 5.7a and 5.7b the adsorbent loadings of both adsorbate components in the highest temperature desorption process (523 K) at multiple reactor locations are presented. Only one desorption process is depicted, as the amount of data from both models is vast, resulting in a number of plots even with only one temperature level. Following that, subfigure 5.7c shows the different adsorbent loading profiles of carbon dioxide for both models at all desorption temperatures at 10% of reactor length.

From subfigure 5.7a it can be seen that the adsorbent loading of carbon dioxide initially rises to values that are significantly above the values achieved in the adsorption process

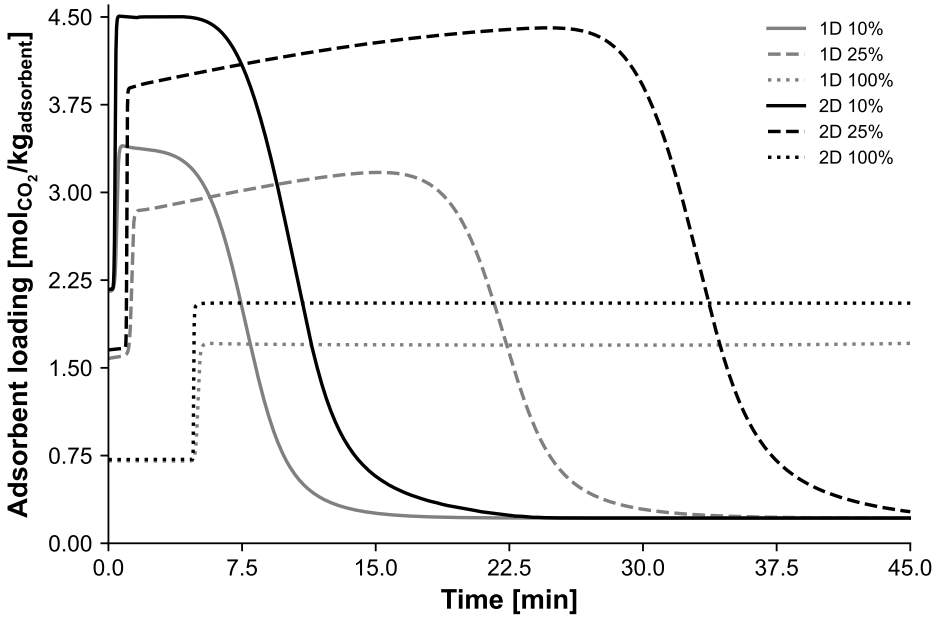

(a) *Desorption step (523 K) adsorbent loading profiles for carbon dioxide.*

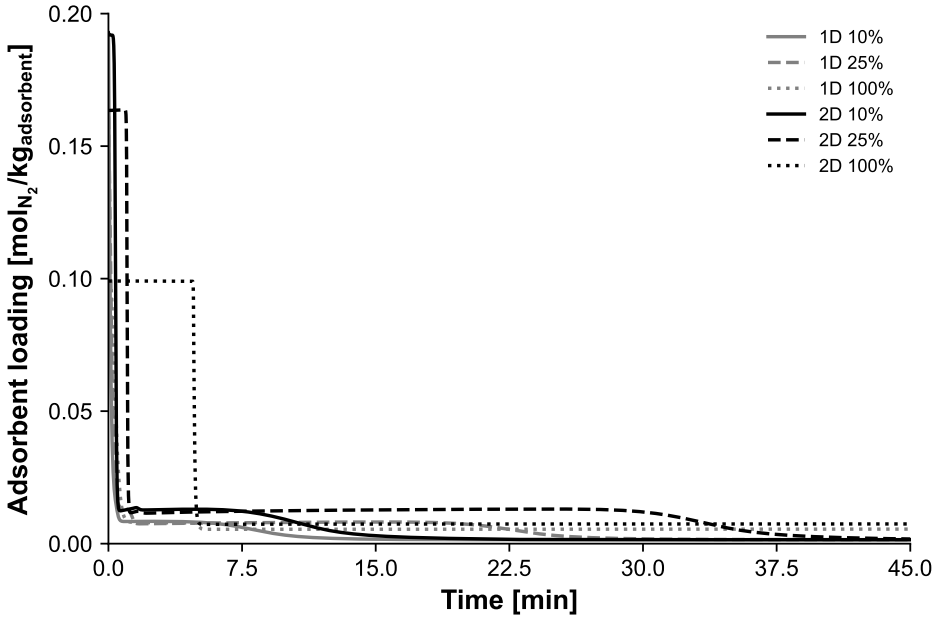

(b) *Desorption step (523 K) adsorbent loading profiles for nitrogen.*

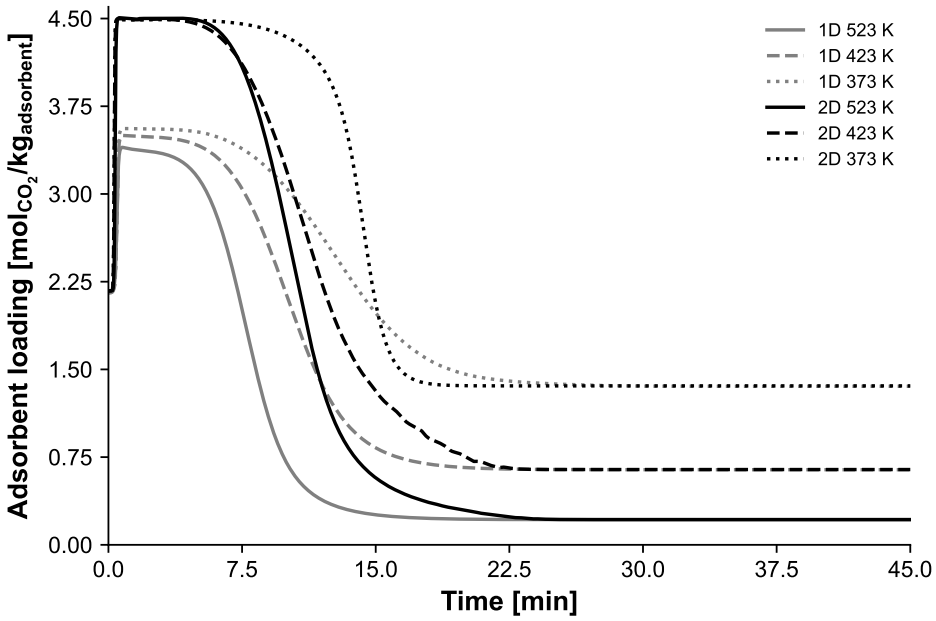

(c) *Adsorbent loading profiles for carbon dioxide 10% of reactor length at all three separate desorption temperatures (indicated in the legend).*

Figure 5.7. *Comparison of one-dimensional and two-dimensional model results in desorption step adsorbent loading profiles. For desorption temperature of 523 K at different axial locations in the reactor for carbon dioxide in subfigure 5.7a and for nitrogen in subfigure 5.7b and for desorption temperatures 373 K, 423 K and 523 K at 10% of reactor length in subfigure 5.7c.*

step. The differences in the adsorbent loading peak and subsequent desorption times between the 1D and 2D models are very significant in the locations at 10% and 25% of reactor length, while at 100% reactor length the extensive desorption phenomenon is yet to occur. Similar behavior can be seen in nitrogen loading (subfigure 5.7b) but as the magnitude of nitrogen loading compared to carbon dioxide is very small, the differences in the results between the two models are not as significant.

The comparison of carbon dioxide adsorbent loading at the three different desorption temperatures between the two models, depicted in subfigure, 5.7c shows similar results also for other desorption temperature levels. More importantly, the variation of the reached minimum adsorbent loading shows great dependence on the desorption temperature. Taking into consideration the achieved maximum adsorbent loading in the adsorption step, the chosen desorption temperature level can have a significant effect on the amount of product carbon dioxide recovered. In general, reaching the peak adsorbent loading and the following desorption also to occur slower in the 2D model compared to the 1D model. In addition, there is no variation in the initial peak loading in the 2D model results, whereas in the 1D model results the initial peak loading show variation with different desorption temperatures. The numerical inaccuracy in the 2D model can affect the temperature dependence of the desorption phenomenon. Also, as mentioned before, the definition of temperature in the models can impact the results.

A comparison of the temperature levels is presented in figure 5.8. Subfigure 5.8a depicts the temperature levels of both models at three separate reactor locations for both models, while subfigure 5.8b provides information on the differences between the models at a certain location in the reactor for all three desorption temperatures. Similarly to the adsorbent loading plots presented in the previous figure, the temperature levels follow a similar trend. Reaching the ultimate desorption temperature takes considerably longer in the 2D model, but both models tend to reach the initial inlet temperature also in the reactor. Subfigure 5.8a only depicts this phenomenon at 10% of reactor length for both models, but the temperature at 25% of reactor length and other locations in the reactor exhibit similar behavior.

The combined adsorbent loading (for carbon dioxide) and temperature profiles for a more clear depiction of the effect of temperature on the desorption phenomenon are presented in figure 5.9. For clarity, the results of the two models are presented in separate subfigures due to the sheer amount of plots required. For both models, the variation of the final reached adsorbent loading at different desorption temperatures is very clear. Even though the effect of temperature is depicted at one location in the reactor, similar phenomenon is expected to occur within the whole reactor as the desorption process progresses. This is a very clear indication of the fact that the choice of desorption temperature has a vast effect on the adsorption process and especially the recovery efficiency of the desired product component.

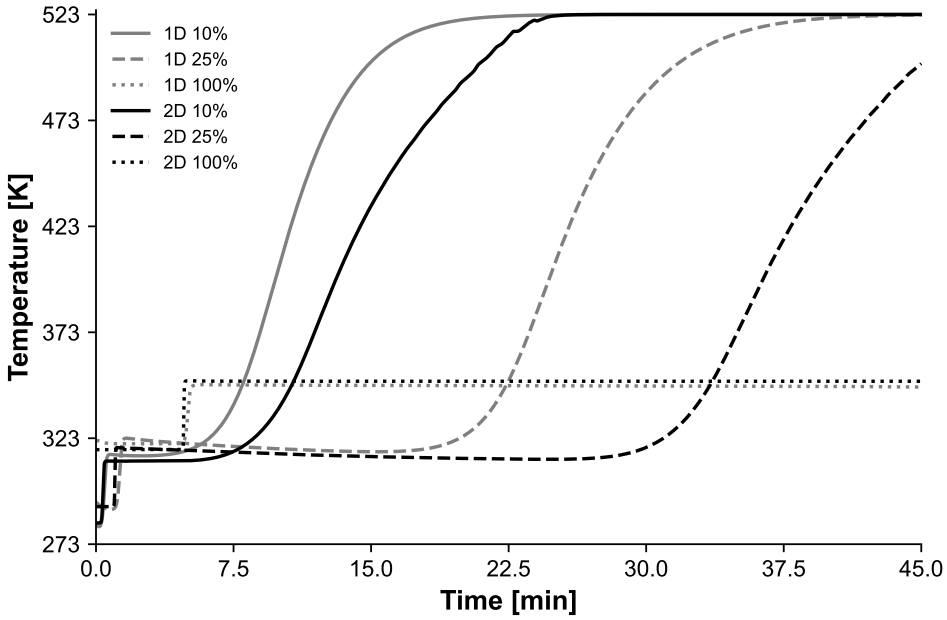

(a) *Desorption step (523 K) temperature profiles at three reactor locations (indicated in the legend).*

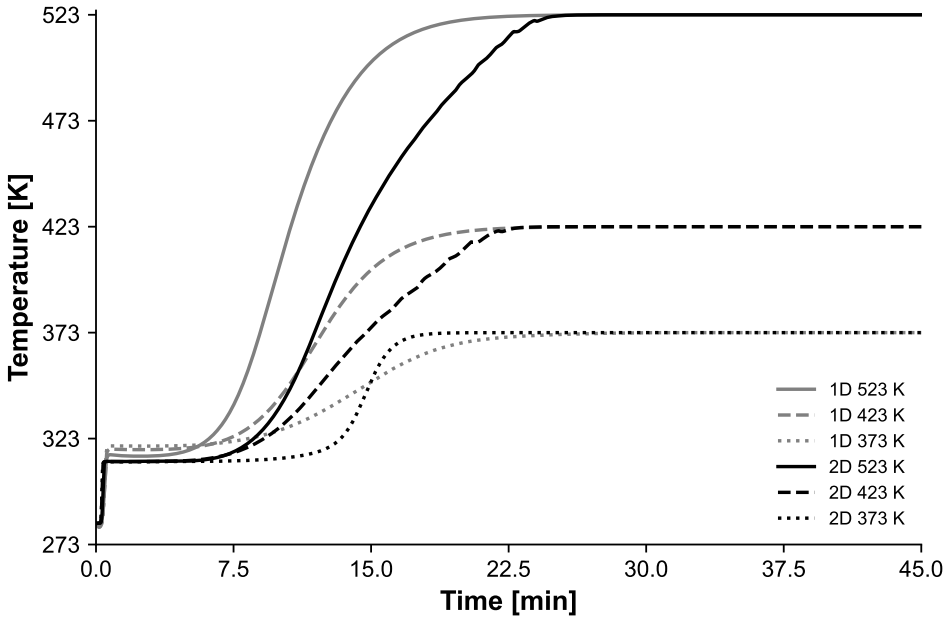

(b) *Temperature profiles for three separate desorption temperatures (indicated in the legend).*

Figure 5.8. *Temperature plots at desorption temperature of 523 K at multiple locations along the reactor and all three separate desorption temperatures at 10% of reactor length. Both models included.*

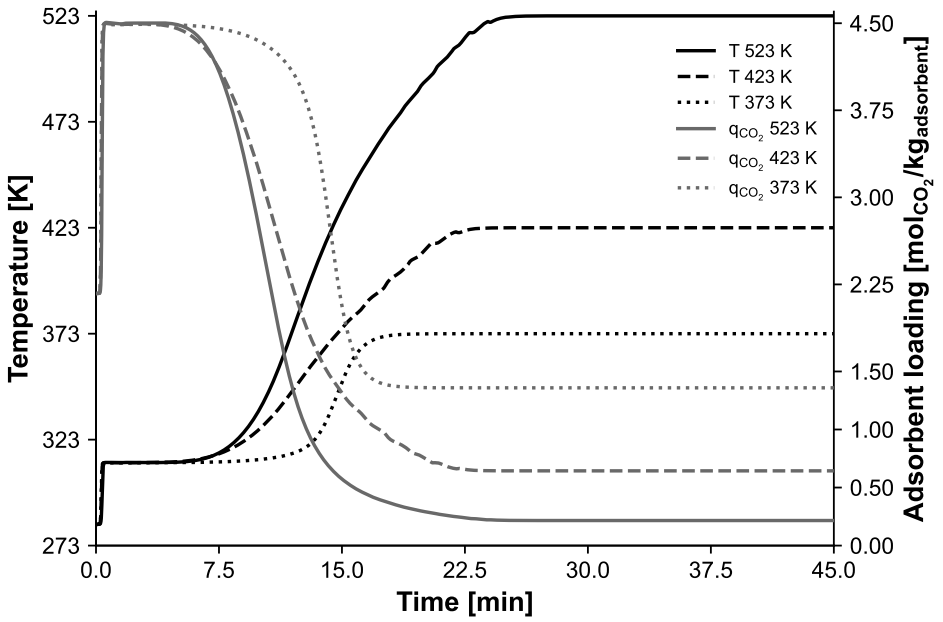

(a) *Adsorbent carbon dioxide loading in desorption at different desorption temperature levels for the two-dimensional model.*

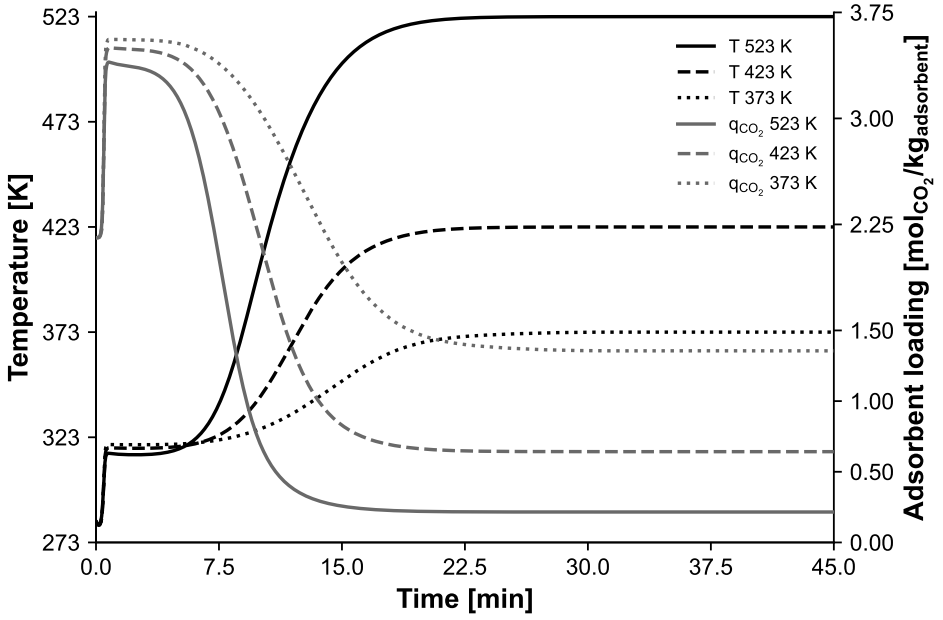

(b) *Adsorbent carbon dioxide loading in desorption at different desorption temperature levels for the one-dimensional model.*

Figure 5.9. *A plot of temperature and adsorbent loading of carbon dioxide for both models, depicting the effect of temperature on adsorbent loading. The data is gathered at 10% of reactor length. Note that the y-axis on the right side is in different scale in the subfigures.*

The difference in initial carbon dioxide adsorbent loadings between the models in the desorption step was deemed to be too large to ignore and it was further inspected. The first 60 seconds of the desorption step at 523 K after the 45 minute adsorption step was simulated with four different time step sizes in the 2D model. The results of this are depicted in figure 5.10.

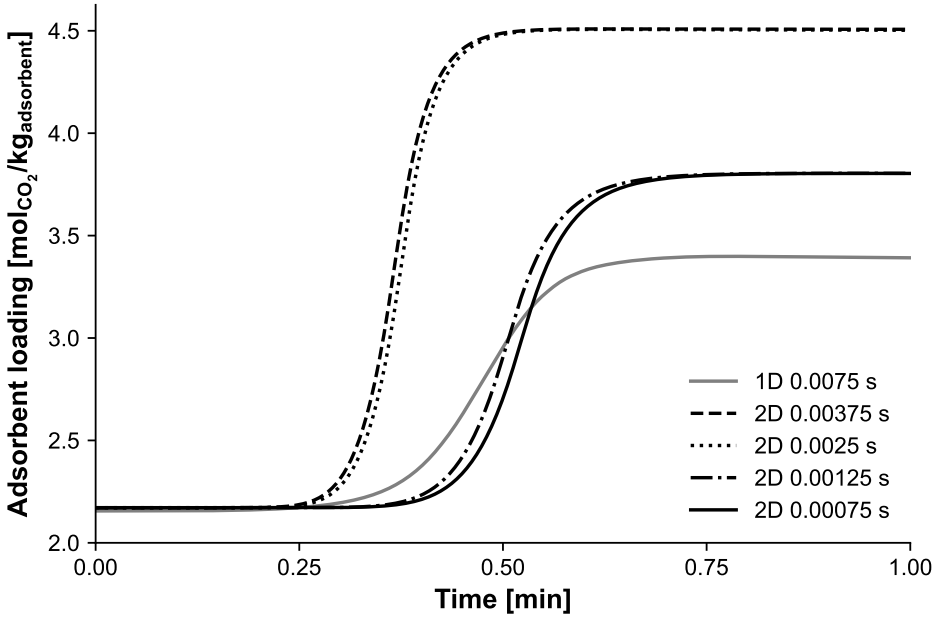

Figure 5.10. *Carbon dioxide adsorbent loading profile in the first 60 seconds of the desorption step at 523 K for four separate time step sizes in the 2D model with the 1D model results included for reference.*

In a similar manner to the mesh independence results (figure 5.1), the behaviour of the desorption process is strongly dependent on the time step size. The two largest time step sizes behave similarly, as do the two smallest ones. However, none of the tested time step sizes could achieve a similar adsorbent loading profile of the 1D model. As no experimental data was available for verification purposes, no clear statement can be said about the reliability of either model. However, the 1D model was not as time step dependent as the 2D model and similar results were gathered with a number of different time step sizes and cell counts in the model development phase.

5.5 Adsorption-desorption cycle

For a more comprehensive depiction of the modelled adsorption-desorption cycle within the whole reactor, figure 5.11 presents the total mean adsorbent loading of carbon dioxide and nitrogen in the whole reactor.

As subfigure 5.11a exhibits, the adsorbent bed loading peak of carbon dioxide in desorption step vastly exceeds the achieved total adsorbent loading in the adsorption step. As

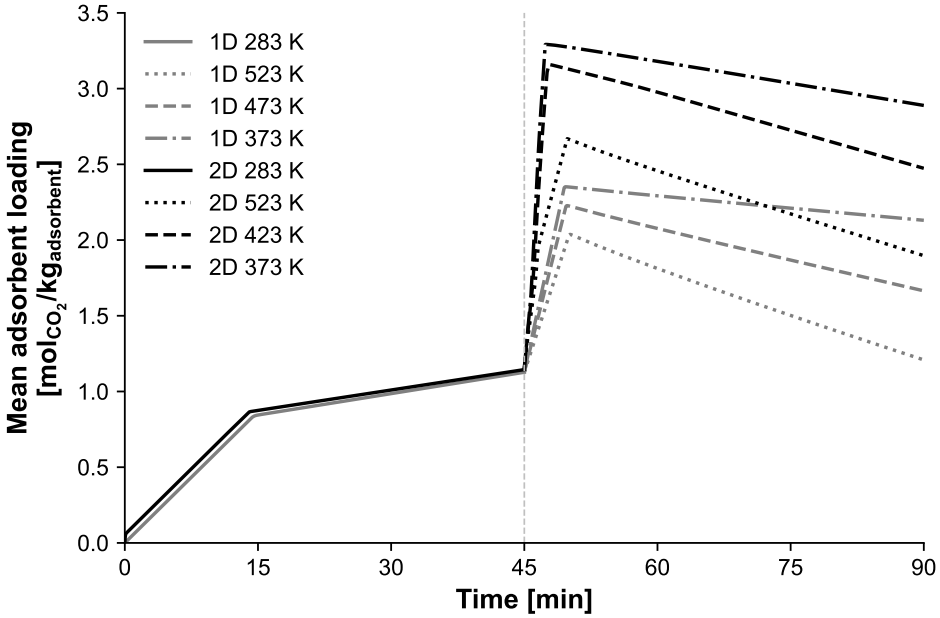

(a) *Total average adsorbent bed loading profile for carbon dioxide during the 1D and 2D process cycles.*

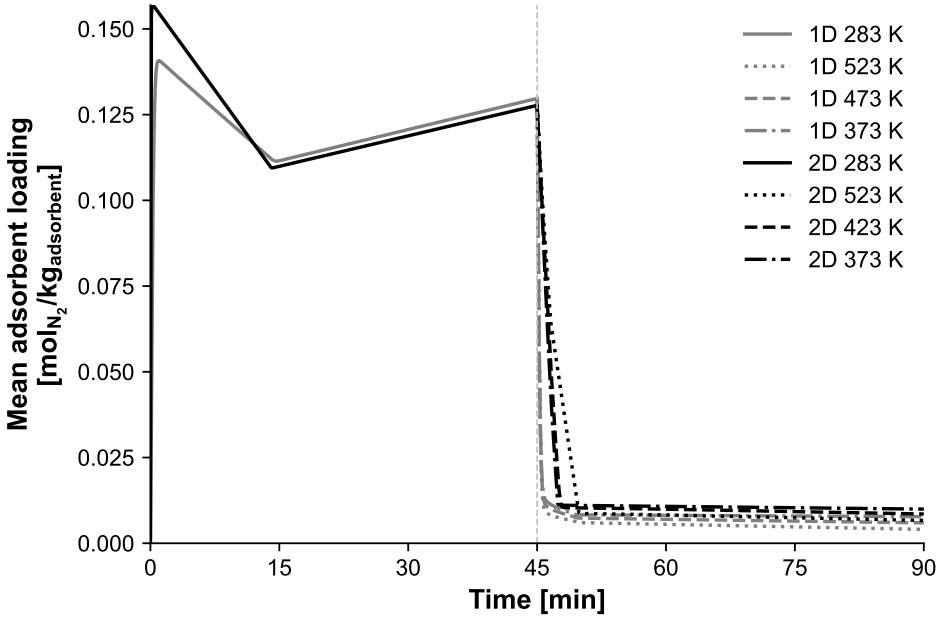

(b) *Total average adsorbent bed loading profile for nitrogen during the 1D and 2D process cycles.*

Figure 5.11. *Reactor total average adsorbent bed loading profiles during the adsorption (283 K) and desorption (373 K, 423 K and 523 K) steps for carbon dioxide and nitrogen. Results from both models included. Model and inlet gas temperature level indicated in the legend.*

the adsorption step was cut off prematurely, this effect is exaggerated and clearly visible. The initial peak loading is caused by the higher carbon dioxide content of the desorption gas and initial low temperature region in the region near the reactor inlet. However, as the higher temperature region caused by the desorption gas flow proceeds in the reactor, the adsorbent loading starts to decrease, as expected. Neither model reaches lower mean adsorbent loading of carbon dioxide in the desorption step compared to the adsorption step, but the desorption trendlines suggest that minimum bed loading would be reached if the desorption step had proceeded for a longer time. As witnessed in subfigure 5.7c, the higher peak loadings of carbon dioxide achieved in the 2D model are also visible in the total mean adsorbent loading plots. Nitrogen loading, depicted in subfigure 5.11b, quickly decreases in both models due to the lower nitrogen content of the desorption gas.

The adsorbent bed loading profiles at the end of each modelled process step from the 2D model are depicted in figure 5.12. The flow direction in these figures is from left to right. The concept of a MTZ, introduced in section 2.5, is visible here. In the adsorption step, the MTZ can be considered to be the transitional region from a higher to a lower loading value. In desorption, this is the opposite as mass is transferred from the adsorbent to the fluid. The adsorbent loading profiles and the location of the MTZ vary slightly between the different desorption temperatures. This is most likely caused by the varying velocity profiles and mass transfer properties between the separate temperature levels.

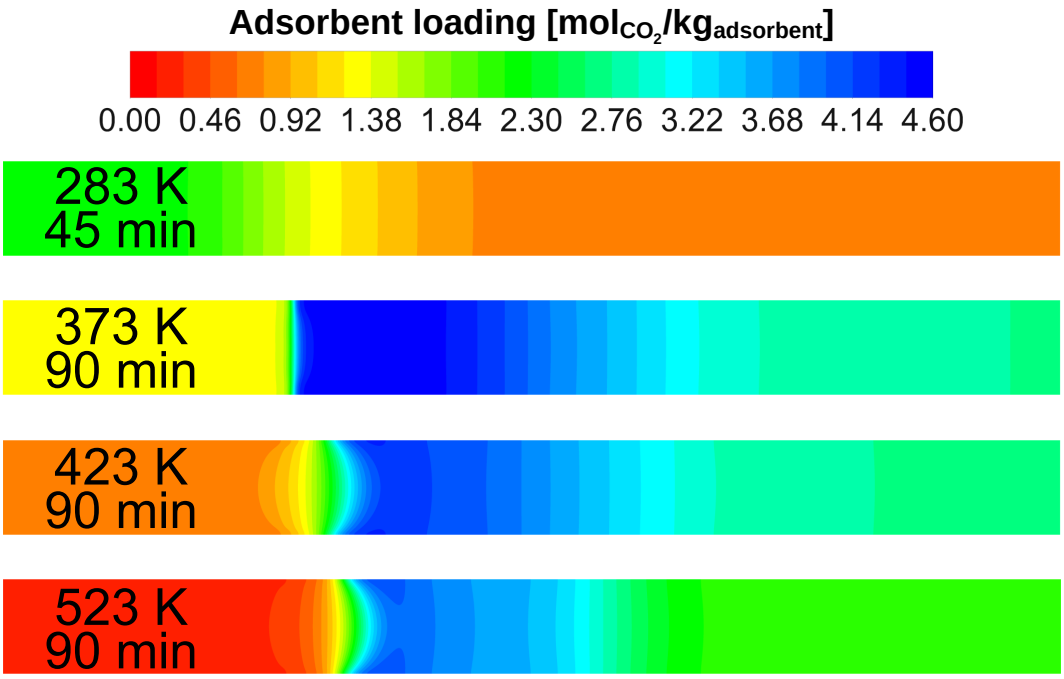

Figure 5.12. *Carbon dioxide adsorbent loading profile in the bed at the end of the adsorption step (283 K) and the desorption steps (373 K, 423 K and 523 K). A mass transfer zone for desorption can be seen from the figures in the areas where adsorbent loading changes substantially. Figures from Ansys Fluent.*

Further inspection of the desorption step at 523 K is presented in figure 5.13, which depicts the variation of pressure and velocity during the process. In addition, the mass source term for carbon dioxide is included. The figures were chosen at this temperature due to the highest variation from ambient temperature in order to maximize potential gradients. Whereas in the 1D model the pressure and velocity are constants, in the 2D model they vary. The pressure profile shows very little variation from the operating pressure of 101 325 Pa, with the highest value being around 101 625 Pa. Velocity profile, however, shows larger variation. In the regions of low adsorbent loading the velocity is higher and vice versa. The inlet velocity of 0.42 $m\,s^{-1}$ decreases down to approximately 0.27 $m\,s^{-1}$ around the MTZ regions as depicted in subfigure 5.7c. This could also be a factor in the variation of the desorption results between the two models. As expected, the carbon dioxide mass source term coincides with the MTZ region presented in figure 5.12. Negative values indicate adsorption while positive values indicate desorption.

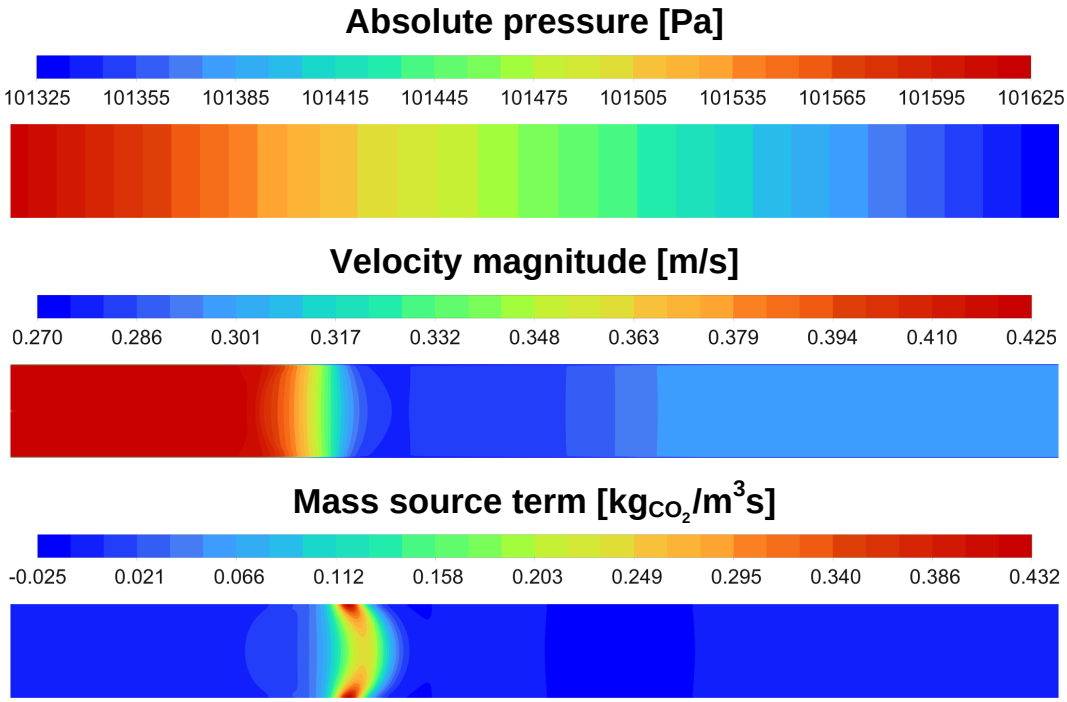

Figure 5.13. *Pressure, velocity and carbon dioxide mass source term profiles in the reactor at the end of the desorption step at 523 K. Pressure profile exhibits slight variation while a larger gradient is witnessed in the velocity profile. Positive mass source term values indicate desorption. Figures from Ansys Fluent.*

The achieved adsorption maximum and desorption minimum adsorbent loading values for both components are presented in table 5.1. As the analysis of the results so far have also shown, a very good agreement with the theoretical values is reached with both models. All the theoretical values are reached in the 1D model. Marginal differences are visible in the 2D model results, which can be accounted to numerical inaccuracy and the slight variation of the operating pressure within the process cycle, which in turn affects the adsorbent loading capacity. Even if the desorption step carbon dioxide adsorbent loading

Table 5.1. *Adsorption maximum and desorption minimum adsorbent loading values achieved by the end of each process step. Theoretical values are calculated at the pressure of 101 325 Pa.*

Component	Adsorbent loading [$mol_i\ kg^{-1}_{adsorbent}$]			
	Adsorption (283 K)	**Desorption (373 K)**	**Desorption (423 K)**	**Desorption (523 K)**
Carbon dioxide				
Theoretical value	*2.163*	*1.356*	*0.642*	*0.215*
1D achieved	2.163	1.356	0.642	0.215
2D achieved	2.173	1.358	0.644	0.216
Nitrogen				
Theoretical value	*0.192*	*0.006*	*0.003*	*0.001*
1D achieved	0.192	0.006	0.003	0.001
2D achieved	0.193	0.006	0.003	0.002

peak results between the model varied, both models are capable of eventually reaching satisfactory adsorbent loading levels and, with improvements, the models could be used for adsorption process cycle modelling.

6. DISCUSSION AND CONCLUSIONS

Energy production has been a major source of carbon dioxide emissions for a very long time and with climate change being a major challenge of the 21st century, mitigation measures are needed more than ever. Carbon capture is one of possible technologies in reducing the impact in the prevailing, combustion-heavy field of energy production. As current absorption-based post-combustion carbon capture technologies have not been proven to be a reliable way for carbon capture, new solutions are needed. Adsorption-based carbon capture has been noted to be one of possible future technologies for this. The very objective of this thesis was to construct and formulate calculation models for the purpose of modelling the reactor in a novel thermal swing adsorption process for carbon dioxide capture from a gas stream resembling a heat and power plant flue gas.

As the scope of this thesis was set strictly on the modelling task, the viability analysis of thermal swing adsorption for carbon capture was not a point of interest. However, as the aspirations for modelling stem from the potential ultimate goal of an industrial implementation of the process, it can not be completely disregarded. While adsorption is utilized in many industrial applications and is very much a mature technology, it is currently still only at research level in post-combustion carbon capture related utilization. The general requirements set on the carbon capture adsorption process from flue gas, regardless of the desorption method, are vast and difficult and there are many obstacles to overcome before industrial-scale processes are to be implemented.

Thermal swing adsorption method does generally tolerate flue gas impurities rather well in comparison to other adsorption processes. Therefore, a throughout flue gas treatment process before carbon capture should in most cases be enough to provide a suitable flue gas stream for the adsorption process. However, related modelling work should also include the consideration of impurities in the gas flow. Impurities were omitted in this work due to lack of proper isotherm data. Various studies have been conducted on the effect of impurities on adsorption processes, but very few include both experimental and modelling work. Future research could combine these two, as studying the effect of impurities in detail would give a more comprehensive look on the topic.

The extensive timescales of thermal swing adsorption processes, as demonstrated in this thesis, are also a big consideration. This fact has been recognized, with a lot of research

concentrating on alternative adsorption processes, namely pressure and vacuum swing adsorption, in which the desorption timescales are considerably shorter. However, from an energy requirement standpoint, as heat required by desorption in a thermal swing process is often economically available in a heat and power plant enviroment, thermal swing adsorption can provide to be a suitable technology for such applications. However, a great amount of research is still needed, especially in the context of comprehensive process modelling and optimization.

Even if the volumetric flows of flue gases vary depending on the energy production method and capacity, the amounts are large nonetheless. The sizes of the experimental reactors in research have, in general, been small and the upscaling is yet to be done. Even though no experimental data was available in this thesis, the modelled reactor is still a step forward from the millimeter scale reactors, albeit still being very moderate in size. However, upscaling even to pilot-scale reactors will require extensive research and experimentation on the topic.

All in all, numerous challenges exist in thermal swing adsorption -based post-combustion carbon capture and further research is required in its many aspects before it is a viable to be implemented into an actual energy production system. Considering the major drawbacks, the technology is most likely a suitable method for capturing a portion of the carbon dioxide emissions from energy production. A potential scenario for successful implementation could include an on-site utilization method of the captured carbon dioxide.

As for the contents of this thesis, an answer to the first research question was found during the extensive and diverse literature review. As adsorption and desorption are very temperature sensitive phenomena, the according temperature levels in adsorption and desorption play a significant role in the process in terms of adsorption capacity. Temperature can also have an effect on the adsorbent and reactor materials, which was not taken into account in this work. Another key factor in adsorption processes is the adsorbent material used. Adsorbent and its properties can have a fundamental influence on an adsorption process and many factors need to be considered when choosing a suitable adsorbent for the process at hand. In addition, the heat and mass transfer and related resistances between the fluid and adsorbent need to be considered. As they can have a huge influence on the adsorption process dynamics, these factors should not be neglected in adsorption process design.

Important indicators were also recognized in regards to process design. Adsorbent equilibrium data provides valuable information regarding the adsorbent and its properties, especially the adsorption capacity. This data can be used in evaluating the choice of a suitable adsorbent for specific process conditions. Equilibrium data can also serve as a point of comparison with actual data gathered from processes. Breakthrough concentration and curves can be used analyze adsorbent performance. The point when the

adsorption step of a process is terminated can be chosen accordingly at a desired point before or after breakthrough starts to occur, based on the nature of the process and the needs related to it. Adsorbent loading is a key indicator in process design and, when coupled with isotherm data, can be used to evaluate process performance especially in modelling work. It ultimately provides a clear indicator of process feasibility.

The models were built upon the literature reviews while the aforementioned process parameters and indicators were utilized in analyzing the modelling results. The comparison of the modelling results with similar studies provided the affirmation that the models can be utilized in adsorption reactor modelling. When the results of the one-dimensional and two-dimensional models were compared, good agreement was found within the results in the adsorption step. Rather significant differences were found in the desorption step, namely the higher initial peak adsorbent loading of carbon dioxide in the two-dimensional model, which was accounted to be due to numerical inaccuracy. This also resulted in longer desorption times for the two-dimensional model. Otherwise, the built reactor models represent an adsorption process and results of the adsorption step can be compared. Thus, an answer to the second research question is provided.

The effect of desorption temperature was also examined in the results analysis, providing an answer to the third research question. With higher temperatures, lower adsorbent loadings can be reached, which leads to more carbon dioxide recovered in a process cycle. Desorption temperature is a key consideration in the design of an adsorption process. While desorption is more effective with higher temperatures, it leads to a higher energy cost and can potentially be a detriment to the adsorbent properties. The choice of a suitable desorption temperature level needs to be scrutinized in actual process design.

In regards to future studies in the area, the choice of an appropriate calculation model depends on the objectives and aims. Both models should include improvements before a more in-depth and scientific approach is taken. The adsorbent bed resistance effects can be included in the one-dimensional model, so that the pressure and velocity gradients are taken into account in the modelling. For computational fluid dynamics calculations, the mesh and time step sizes should be analyzed more rigorously in order to achieve the most favorable conditions for the calculations in terms of computational cost. This is especially true for the desorption step, as the results of the two models exhibited considerable variance. Thus, validation of both of the models in the desorption step is also required.

Another point of consideration for future studies are the adsorption parameters. The isotherm model used in the modelling in this thesis included setting adsorption-related parameters as constants due to lack of more detailed data. The mass transfer coefficients and heats of adsorption were set to be constants which can be a very rough approximation, depending on the process conditions. If proper experimental data is available, a more detailed approximation of the adsorption-related parameters can be made.

For more realistic results, the effect of impurities could also be taken into account.

Even if improvements are recommended in further studies, the models can still be utilized as they stand now, especially in the adsorption step. The one-dimensional model can be used to vary process parameters and conditions with quick results. It can also serve as a convenient way of finding suitable isotherm models for different components that correspond to the actual experimental adsorption process. When suitable isotherm models are found, depending on the size of the reactor in which experiments are conducted, the Ansys Fluent model can be a viable option for verifying the experimental data in a more sophisticated manner. This is especially true for small-scale reactors, as done in previous studies. In order to study and model the desorption step, more research is needed in order to pinpoint the reasons for variance between the two models and to verify the reliability of the models.

For more comprehensive modelling of larger reactors, constructing a two-dimensional Python model could be an appropriate approach, offering a computational cost controlled modelling tool with highly extensive modification and adjustment capabilities for a multitude of modelling needs and desires. Especially if a number of complete adsorption-desorption cycles are to be modelled, computational cost will become a key consideration as the modelling times will lengthen extensively.

In short, the main takeaways from this thesis are:

- The simple one-dimensional Python-based model is capable of modelling the phenomena and behavior of the adsorption step in a thermal swing adsorption reactor.
- The above also applies to the two-dimensional Ansys Fluent model, but it requires the implementation of user-defined functions in order to be a viable tool for modelling the aforementioned reactor.
- The adsorption step results from the two models are comparable, but due to numerical inaccuracy and possibly other factors, the two-dimensional model results exhibit variation when compared to the one-dimensional model in the desorption step.
- Desorption temperature is a key consideration in adsorption process design, as it plays a crucial role in the process dynamics and product recovery.
- The constructed models can be utilized in modelling of the adsorption step as they are now, but for the purposes of future research the models should be improved and further developed for better representation of reactor behavior. This is especially true when considering the modelling of desorption, which requires model validation.
- A two-dimensional Python-based model could be a viable option for a future modelling tool with vast modification capabilities and a lower computational cost compared to a computational fluid dynamics model.

REFERENCES

Abd, A. A., Naji, S. Z., Hashim, A. S. & Othman, M. R. (2020). Carbon dioxide removal through physical adsorption using carbonaceous and non-carbonaceous adsorbents: A review. *Journal of Environmental Chemical Engineering* 8.5, pp. 104–142. ISSN: 2213-3437. DOI: 10.1016/j.jece.2020.104142. URL: https://www.sciencedirect.com/science/article/pii/S2213343720304905.

Anchondo, C. (2022). *CCS 'red flag?' World's sole coal project hits snag*. E&E News. URL: https://www.eenews.net/articles/ccs-red-flag-worlds-sole-coal-project-hits-snag/ (visited on 20.2.2023).

Anderson, R. A. (1977). Adsorption, General. *Encyclopedia of Chemical Processing and Design 2 - Additives to Alpha*. Ed. by J. J. McKetta & W. A. Cunningham. Marcel Dekker, Inc., pp. 174–213. ISBN: 0-8247-2452-6.

ANSYS, Inc. (2022a). *Ansys Fluent Customization Manual*. Available through Ansys Fluent software (version 2022R1).

ANSYS, Inc. (2022b). *Ansys Fluent Theory Guide*. Available through Ansys Fluent software (version 2022R1).

ANSYS, Inc. (2022c). *Ansys Fluent User's Guide*. Available through Ansys Fluent software (version 2022R1).

Bahadori, A. (2012). Prediction of Axial Dispersion in Plug-Flow Reactors Using a Simple Method. *Journal of Dispersion Science and Technology* 33.2, pp. 200–205. ISSN: 0193-2691. DOI: 10.1080/01932691.2011.561159. URL: https://doi.org/10.1080/01932691.2011.561159.

Barbato, M. & Bruno, C. (1996). Heterogeneous Catalysis: Theory, Models and Applications. *Molecular Physics and Hypersonic Flows*. Ed. by M. Capitelli, pp. 139–160. ISBN: 978-94-010-6604-4. DOI: 10.1007/978-94-009-0267-1_8.

Bastos-Neto, M., de Azevedo, D. C. S. & de Lucena, S. M. P. (2020). Adsorption. *Kirk-Othmer Encyclopedia of Chemical Technology*. John Wiley & Sons, Ltd., pp. 1–59. ISBN: 978-0-471-23896-6. DOI: 10.1002/0471238961.0104191518212008.a01.pub3.

Bell, I. H., Wronski, J., Quoilin, S. & Lemort, V. (2014). Pure and Pseudo-pure Fluid Thermophysical Property Evaluation and the Open-Source Thermophysical Property Library CoolProp. *Industrial & Engineering Chemistry Research* 53.6, pp. 2498–2508. DOI: 10.1021/ie4033999. URL: http://pubs.acs.org/doi/abs/10.1021/ie4033999.

Ben-Mansour, R., Basha, M. & Qasem, N. A. A. (2017). Multicomponent and multi-dimensional modeling and simulation of adsorption-based carbon dioxide separation. *Computers & chemical engineering* 99, pp. 255–270. ISSN: 0098-1354. DOI: 10.1016/j.compchemeng.2017.01.040.

Ben-Mansour, R., Abuelyamen, A. & Qasem, N. A. (2020). Thermal design and management towards high capacity CO2 adsorption systems. *Energy conversion and management* 212, pp. 112796–. ISSN: 0196-8904. DOI: 10.1016/j.enconman.2020.112796.

Ben-Mansour, R., Qasem, N. A. & Antar, M. A. (2018). Carbon dioxide adsorption separation from dry and humid CO2/N2 mixture. *Computers & chemical engineering* 117, pp. 221–235. ISSN: 0098-1354. DOI: 10.1016/j.compchemeng.2018.06.016.

Between the Buried and Me (2009). Swim to the Moon. *The Great Misdirect*.

Boumghar, S., Bedel, S., Sigot, L. & Vallières, C. (2020). Adsorption of CO2 in presence of NOx and SOx on activated carbon textile for CO2 capture in post-combustion conditions. *Adsorption* 26.7, pp. 1173–1181. ISSN: 1572-8757. DOI: 10.1007/s10450-020-00207-6. URL: https://doi.org/10.1007/s10450-020-00207-6.

Chao, C., Deng, Y., Dewil, R., Baeyens, J. & Fan, X. (2021). Post-combustion carbon capture. *Renewable and Sustainable Energy Reviews* 138, p. 110490. ISSN: 1364-0321. DOI: 10.1016/j.rser.2020.110490. URL: https://www.sciencedirect.com/science/article/pii/S1364032120307760.

Dantas, T. L. P., Luna, F. M. T., Silva, I. J., Azevedo, D. C. S. de, Grande, C. A., Rodrigues, A. E. & Moreira, R. F. P. M. (2011). Carbon dioxide–nitrogen separation through adsorption on activated carbon in a fixed bed. *Chemical Engineering Journal* 169.1, pp. 11–19. ISSN: 1385-8947. DOI: 10.1016/j.cej.2010.08.026. URL: https://www.sciencedirect.com/science/article/pii/S138589471000731X.

Froment, G. F., Bischoff, K. B. & Wilde, J. D. (2010). Chapter 12: Complex Flow Patterns. *Chemical Reactor Analysis and Design*. 3rd ed. John Wiley & Sons, Incorporated, pp. 639–718. ISBN: 978-1-118-13653-9.

Hwang, K. S., Jun, J. H. & Lee, W. K. (1995). Fixed-bed adsorption for bulk component system. Non-equilibrium, non-isothermal and non-adiabatic model. *Chemical Engineering Science* 50.5, pp. 813–825. ISSN: 0009-2509. DOI: 10.1016/0009-2509(94)00433-R. URL: https://www.sciencedirect.com/science/article/pii/000925099400433R.

IEA Bioenergy (2023). *Implementation of bioenergy in Finland – 2021 update*. URL: https://www.ieabioenergy.com/wp-content/uploads/2021/11/CountryReport2021_Finland_final.pdf (visited on 11.8.2023).

IEAGHG (2019). *Towards Zero Emissions CCS in Power Plants Using Higher Capture Rates or Biomass - IEAGHG Technical Report 2019-02*. URL: https://ieaghg.org/

publications/technical-reports/reports-list/9-technical-reports/951-2019-02-towards-zero-emissions.

Iisa, K. (1995). 10. Rikin oksidien muodostuminen ja poistaminen. *Poltto ja palaminen*. Ed. by R. Raiko, I. Kurki-Suonio, J. Saastamoinen & M. Hupa. 1st ed. International Flame Research Foundation (IFRF) Suomen kansallinen osasto, pp. 277–297. ISBN: 951-666-448-2.

International Energy Agency (2023a). *About CCUS*. URL: https://www.iea.org/reports/about-ccus (visited on 14.8.2023).

International Energy Agency (2023b). *Greenhouse Gas Emissions from Energy Data Explorer*. URL: https://www.iea.org/data-and-statistics/data-tools/greenhouse-gas-emissions-from-energy-data-explorer (visited on 11.8.2023).

Jiang, L., Wang, R. Q., Gonzalez-Diaz, A., Smallbone, A., Lamidi, R. O. & Roskilly, A. P. (2020). Comparative analysis on temperature swing adsorption cycle for carbon capture by using internal heat/mass recovery. *Applied Thermal Engineering* 169, p. 114973. ISSN: 1359-4311. DOI: 10.1016/j.applthermaleng.2020.114973. URL: https://www.sciencedirect.com/science/article/pii/S1359431119373181.

Jribi, S., Miyazaki, T., Saha, B. B., Pal, A., Younes, M. M., Koyama, S. & Maalej, A. (2017). Equilibrium and kinetics of CO2 adsorption onto activated carbon. *International Journal of Heat and Mass Transfer* 108, pp. 1941–1946. ISSN: 0017-9310. DOI: 10.1016/j.ijheatmasstransfer.2016.12.114. URL: https://www.sciencedirect.com/science/article/pii/S0017931015306372.

Kapoor, A. & Yang, R. T. (1987). Roll-up in fixed-bed, multicomponent adsorption under pore-diffusion limitation. *AIChE Journal* 33.7, pp. 1215–1217. ISSN: 1547-5905. DOI: 10.1002/aic.690330717. URL: https://onlinelibrary.wiley.com/doi/abs/10.1002/aic.690330717.

Keller, J. U. & Staudt, R. (2005). Chapter 7: Adsorption Isotherms. *Gas Adsorption Equilibria: Experimental Methods and Adsorptive Isotherms*. 1st ed. Springer US, pp. 359–408. ISBN: 978-1-280-14801-9. DOI: 10.1007/b102056.

Keller II, G. E. & Anderson, R. A. (1987). “Chapter 12. Adsorption”. Rousseau, R. W. *Handbook of Separation Process Technology*. Wiley Interscience Imprint, pp. 644–696. ISBN: 978-1-59124-745-6.

Ketabchi, M. R., Babamohammadi, S., Davies, W. G., Gorbounov, M. & Masoudi Soltani, S. (2023). Latest advances and challenges in carbon capture using bio-based sorbents: A state-of-the-art review. *Carbon Capture Science & Technology* 6, p. 100087. ISSN: 2772-6568. DOI: 10.1016/j.ccst.2022.100087. URL: https://www.sciencedirect.com/science/article/pii/S2772656822000574.

Kilpinen, P. (1995). 9. Typen oksidien muodostuminen ja hajoaminen. *Poltto ja palaminen*. Ed. by R. Raiko, I. Kurki-Suonio, J. Saastamoinen & M. Hupa. 1st ed. International Flame Research Foundation (IFRF) Suomen kansallinen osasto, pp. 239–276. ISBN: 951-666-448-2.

Laidler, K. J., Meiser, J. H. & Sanctuary, B. C. (2003). 18. Surface Chemistry and Colloids. *Physical Chemistry*. 4. ed. Houghton Mifflin Company, pp. 929–965. ISBN: 0-618-12341-5.

Lei, M., Vallieres, C., Grevillot, G. & Latifi, M. A. (2013). Thermal Swing Adsorption Process for Carbon Dioxide Capture and Recovery: Modeling, Simulation, Parameters Estimability, and Identification. *Industrial & Engineering Chemistry Research* 52.22. ISSN: 0888-5885. DOI: 10.1021/ie3029152. URL: https://doi.org/10.1021/ie3029152.

Lian, Y., Deng, S., Li, S., Guo, Z., Zhao, L. & Yuan, X. (2019). Numerical analysis on CO2 capture process of temperature swing adsorption (TSA): Optimization of reactor geometry. *International Journal of Greenhouse Gas Control* 85, pp. 187–198. ISSN: 1750-5836. DOI: 10.1016/j.ijggc.2019.03.029. URL: https://www.sciencedirect.com/science/article/pii/S1750583619300659.

Mattei, S. & Schlissel, D. (2022). *The ill-fated Petra Nova CCS project: NRG Energy throws in the towel*. Institute for Energy Economics and Financial Analysis. URL: https://ieefa.org/resources/ill-fated-petra-nova-ccs-project-nrg-energy-throws-towel (visited on 20.2.2023).

Noll, K. E., Gounaris, V. & Hou, W.-S. (1992a). I. Adsorption as a treatment process. *Adsorption technology for air and water pollution control*. Lewis, pp. 1–20. ISBN: 0-87371-340-0.

Noll, K. E., Gounaris, V. & Hou, W.-S. (1992b). II. Adsorption theory. *Adsorption technology for air and water pollution control*. Lewis, pp. 21–48. ISBN: 0-87371-340-0.

Ntiamoah, A., Ling, J., Xiao, P., Webley, P. A. & Zhai, Y. (2016). CO2 Capture by Temperature Swing Adsorption: Use of Hot CO2-Rich Gas for Regeneration. *Industrial & Engineering Chemistry Research* 55.3, pp. 703–713. ISSN: 0888-5885. DOI: 10.1021/acs.iecr.5b01384. URL: https://doi.org/10.1021/acs.iecr.5b01384.

Osaka, Y., Tsujiguchi, T. & Kodama, A. (2018). Experimental investigation on the CO2 separation performance from humid flue gas by TSA process. *Separation and Purification Technology* 207, pp. 77–82. ISSN: 1383-5866. DOI: 10.1016/j.seppur.2018.06.008. URL: https://www.sciencedirect.com/science/article/pii/S1383586617310080.

Punpee, S. & Phalakornkule, C. (2022). Aspen adsorption simulation for the effects of purge flow rate and vacuum pressure in vacuum pressure swing adsorption. *Materials Today: Proceedings*. 2021 Research, Invention, and Innovation Congress: Materials Science 52, pp. 2517–2522. ISSN: 2214-7853. DOI: 10.1016/j.matpr.2021.10.442. URL: https://www.sciencedirect.com/science/article/pii/S2214785321069509.

Qasem, N. A. A. & Ben-Mansour, R. (2022). Assessment of Appropriate Geometry for Thermally Efficient CO2 Adsorption Beds. *Applied sciences* 12.11, pp. 5726–. ISSN: 2076-3417. DOI: 10.3390/app12115726.

Qasem, N. A. & Ben-Mansour, R. (2018a). Adsorption breakthrough and cycling stability of carbon dioxide separation from CO2/N2/H2O mixture under ambient conditions using 13X and Mg-MOF-74. *Applied energy* 230, pp. 1093–1107. ISSN: 0306-2619. DOI: 10.1016/j.apenergy.2018.09.069.

Qasem, N. A. & Ben-Mansour, R. (2018b). Energy and productivity efficient vacuum pressure swing adsorption process to separate CO2 from CO2/N2 mixture using Mg-MOF-74: A CFD simulation. *Applied energy* 209, pp. 190–202. ISSN: 0306-2619. DOI: 10.1016/j.apenergy.2017.10.098.

Rist, S. & Hartmann, N. (2018). Aquatic Ecotoxicity of Microplastics and Nanoplastics: Lessons Learned from Engineered Nanomaterials. *Handbook of Environmental Chemistry*, pp. 25–49. ISBN: 978-3-319-61614-8. DOI: 10.1007/978-3-319-61615-5_2.

Roy, S. & Moharir, A. S. (2019). Modeling the Generic Breakthrough Curve for Adsorption Process. *arXiv: Applied Physics*. URL: https://www.semanticscholar.org/paper/Modeling-the-Generic-Breakthrough-Curve-for-Process-Roy-Moharir/8ad5e70bee942a6b7a74e44071d70b801f832898.

Ruthven, D. M. (1984a). 1. Microporous adsorbents. *Principles of adsorption and adsorption processes*. John Wiley & Sons, pp. 1–28. ISBN: 0-471-86606-7.

Ruthven, D. M. (1984b). 11. Adsorption separation processes: I. Cyclic batch systems. *Principles of adsorption and adsorption processes*. John Wiley & Sons, pp. 336–379. ISBN: 0-471-86606-7.

Ruthven, D. M. (1984c). 2. Physical adsorption and the characterization of porous adsorbents. *Principles of adsorption and adsorption processes*. John Wiley & Sons, pp. 29–61. ISBN: 0-471-86606-7.

Ruthven, D. M. (1984d). 5. Diffusion in porous media. *Principles of adsorption and adsorption processes*. John Wiley & Sons, pp. 124–165. ISBN: 0-471-86606-7.

Shafeeyan, M. S., Wan Daud, W. M. A. & Shamiri, A. (2014). A review of mathematical modeling of fixed-bed columns for carbon dioxide adsorption. *Chemical Engineering Research and Design* 92.5, pp. 961–988. ISSN: 0263-8762. DOI: 10.1016/j.cherd.2013.08.018. URL: https://www.sciencedirect.com/science/article/pii/S026387621300347X.

Sherman, J. D. (1991). Adsorption, Gas Separation. *Kirk-Othmer Encyclopedia of Chemical Technology - Volume 1*. Ed. by J. I. Kroschwitz & M. Howe-Grant. 4th ed. Kirk-Othmer Encyclopedia of Chemical Technology, pp. 529–572. ISBN: 0-471-52669-X.

The Babcock & Wilcox Company (1972). Section II: Steam generation from chemical energy - 18: Combustion by-products. *Steam/ its generation and use.* 38. ed. Babcock & Wilcox, pp. 1–4.

The International Union of Pure and Applied Chemistry (IUPAC) (2023a). *IUPAC - absorption (A00036)*. DOI: 10.1351/goldbook.A00036. URL: https://goldbook.iupac.org/terms/view/A00036 (visited on 24.1.2023).

The International Union of Pure and Applied Chemistry (IUPAC) (2023b). *IUPAC - desorption (D01620)*. DOI: 10.1351/goldbook.D01620. URL: https://goldbook.iupac.org/terms/view/D01620 (visited on 24.1.2023).

The SciPy Community (2023). *scipy.integrate.solve_ivp — SciPy v1.10.1 Manual*. URL: https://docs.scipy.org/doc/scipy/reference/generated/scipy.integrate.solve_ivp.html (visited on 14.6.2023).

Thomas, J. M. (1961). The existence of endothermic adsorption. *Journal of chemical education* 38.3, pp. 138–139. ISSN: 0021-9584. DOI: 10.1021/ed038p138.

Thomas, W. J. & Crittenden, B. D. (1998a). 2. Adsorbents. *Adsorption technology and design*. Butterworth-Heinemann, pp. 8–30. ISBN: 978-1-281-00595-3.

Thomas, W. J. & Crittenden, B. D. (1998b). 3. Fundamentals of adsorption equilibria. *Adsorption technology and design*. Butterworth-Heinemann, pp. 31–65. ISBN: 978-1-281-00595-3.

Thomas, W. J. & Crittenden, B. D. (1998c). 4. Rates of adsorption of gases and vapours by porous media. *Adsorption technology and design*. Butterworth-Heinemann, pp. 66–95. ISBN: 978-1-281-00595-3.

Thomas, W. J. & Crittenden, B. D. (1998d). 5. Processes and cycles. *Adsorption technology and design*. Butterworth-Heinemann, pp. 98–134. ISBN: 978-1-281-00595-3.

Thomas, W. J. & Crittenden, B. D. (1998e). 6. Design procedures. *Adsorption technology and design*. Butterworth-Heinemann, pp. 135–186. ISBN: 978-1-281-00595-3.

Thommes, M., Kaneko, K., Neimark, A. V., Olivier, J. P., Rodriguez-Reinoso, F., Rouquerol, J. & Sing, K. S. (2015). Physisorption of gases, with special reference to the evaluation of surface area and pore size distribution (IUPAC Technical Report). *Pure and applied chemistry* 87.9, pp. 1051–1069. ISSN: 0033-4545. DOI: 10.1515/pac-2014-1117.

Virtanen, P., Gommers, R., Oliphant, T. E., Haberland, M., Reddy, T., Cournapeau, D., Burovski, E., Peterson, P., Weckesser, W., Bright, J., van der Walt, S. J., Brett, M., Wilson, J., Millman, K. J., Mayorov, N., Nelson, A. R. J., Jones, E., Kern, R., Larson, E., Carey, C. J., Polat, İ., Feng, Y., Moore, E. W., VanderPlas, J., Laxalde, D., Perktold, J., Cimrman, R., Henriksen, I., Quintero, E. A., Harris, C. R., Archibald, A. M., Ribeiro, A. H., Pedregosa, F., van Mulbregt, P. & SciPy 1.0 Contributors (2020). SciPy 1.0: Fun-

damental Algorithms for Scientific Computing in Python. *Nature Methods* 17, pp. 261–272. DOI: 10.1038/s41592-019-0686-2.

Wilcox, J. (2012). 1. Introduction to Carbon Capture. *Carbon Capture*. 1st ed. Springer New York, pp. 1–34. ISBN: 978-1-4614-2215-0. DOI: 10.1007/978-1-4614-2215-0.

Wilkes, M. D. & Brown, S. (2022). Flexible CO2 capture for open-cycle gas turbines via vacuum-pressure swing adsorption: A model-based assessment. *Energy* 250, p. 123805. ISSN: 0360-5442. DOI: 10.1016/j.energy.2022.123805. URL: https://www.sciencedirect.com/science/article/pii/S0360544222007083.

Ye, F., Xiao, J., Hu, B., Benard, P. & Chahine, R. (2012). Implementation for Model of Adsoptive Hydrogen Storage Using UDF in Fluent. *Physics Procedia*. International Conference on Applied Physics and Industrial Engineering 2012 24, pp. 793–800. ISSN: 1875-3892. DOI: 10.1016/j.phpro.2012.02.118. URL: https://www.sciencedirect.com/science/article/pii/S1875389212001617.